Applied Geochemistry 100 (2019) 104–120

Contents lists available at ScienceDirect

Applied Geochemistry

journal homepage: www.elsevier.com/locate/apgeochem

# Genesis of the South Zhuguang uranium ore field, South China: Fluid inclusion and H–C–O–S–Sr isotopic constraints

Chuang Zhang[a,b,c,*], Yuqi Cai[a,b,c], Qian Dong[a,d], Hao Xu[e], Sheng He[a,b,c]

[a] Beijing Research Institute of Uranium Geology, CNNC, Beijing, 100029, China
[b] Key Lab of Uranium Resource Prospecting and Evaluating Technology, CNNC, Beijing, 100029, China
[c] No.10 Xiaoguandongli, Chaoyang District, Beijing, 100029, China
[d] China University of Geoscience (Beijing), Beijing, 100083, China
[e] China Nuclear Geology, CNNC, Beijing, 100000, China

ARTICLE INFO

Editorial handling by Dr Q Gong

*Keywords:*
Bulk volatiles
Ionic composition
Stable isotopes
Strontium isotopes
Genesis
South Zhuguang uranium ore field

ABSTRACT

The South Zhuguang uranium (U) ore field in South China, which was discovered in the 1950s, contains an estimated > 20,000 t of recoverable U. The U ore is hosted by the Zhuguang granite massif, which is located in the South China Block. The main uranium-bearing mineral, pitchblende, is found mainly in veins along high-angle normal faults, associated with hematite, quartz, fluorite, calcite, and locally pyrite. The hydrothermal alteration is generally silicification, illitization, hematization, and chloritization that developed adjacent to the ore-bearing faults and outwards over hundreds of meters into the unaltered granites.

The ore-forming fluids in the South Zhuguang U ore field can be classified into two stages. Stage I fluids were acidic and oxidizing, with fluoride and sulfate complexes of $UO_2^{2+}$ being the dominant species in the fluid. Stage II fluids were alkaline and oxidizing, with carbonate and hydroxide complexes of $UO_2^{2+}$ being the dominant species. $\delta^{18}O$ values of syn-ore quartz range from +6.29‰ to +14.30‰, with calculated $\delta^{18}O_{W\text{-}SMOW}$ values from −1.85‰ to +5.35‰. $\delta D_{W\text{-}SMOW}$ values of the ore-forming fluids were −104.4‰ to −23.1‰. $\delta^{18}O$ values of the altered granites increase gradually from ~ +4‰ close to ore, to ~ +12‰ in the nearly unaltered granites. The $\delta^{13}C$ and $\delta^{18}O$ values for syn-ore calcite range from −10.3‰ to −4.3‰ and −22.41‰ to −16.8‰ relative to Pee Dee Belemnite, respectively, with calculated $\delta^{18}O$ and $\delta^{13}C$ values for water and $CO_2$ of −2.97‰ to +2.83‰ and −11.2‰ to −5.2‰, respectively. The $\delta^{34}S_{V\text{-}CDT}$ values of syn-ore pyrite range from −17.1‰ to −3.4‰. Initial $^{87}Sr/^{86}Sr$ ratios of syn- and post-ore fluorite vary from 0.719250 to 0.721327 and 0.714598 to 0.716299, respectively.

The ore-forming fluids in the South Zhuguang U ore field were sourced primarily from Cretaceous–Paleogene redbed basins in the south, and initially derived from meteoric waters. Hydrothermal alteration associated with stage I fluids released considerable amounts of $Ca^{2+}$ and $F^-$ into the ore-forming fluids, increased the fluid pH, decreased the stability of the dominant fluoride complexes, and lowered the saturation solubility of the uranyl ions. Reduction of the ore-forming fluid converted $U^{6+}$ into $U^{4+}$, which resulted in the deposition of pitchblende–fluorite–quartz veins of the stage I ore in fractures along with pyrite. During stage II, the U mineralization was controlled mainly by $CO_2$ degassing, which resulted in decomposition of the carbonate complex $UO_2(CO_3)^{2-}$, and deposition of U in pitchblende–calcite–quartz veins as the ore-forming fluid was reduced.

## 1. Introduction

The South Zhuguang uranium (U) ore field was discovered in the late 1950s and has been mined for decades. It occurs in the Zhuguang granite massif, which crops out in Guangdong, Jiangxi, and Hunan provinces, South China (Fig. 1; Dahlkamp, 2009; CNG and BRIUG, 2010). The ore field has estimated recoverable U reserves of > 20,000 t (CNG and BRIUG, 2010). Given that the ore-hosting rocks are predominantly granites, this U ore field has always been classified as of the granitic type (e.g., Du et al., 1982; CNG, 2005; Huang et al., 2005). The U ores within the South Zhuguang area are characteristically low-to medium-grade (0.1%–0.5% U) and found at shallow levels (even at the

* Corresponding author. Building No.294, Furongyuan, Tongzhou District, Beijing City, China.
*E-mail addresses:* zhangc198506@126.com (C. Zhang), caiyq1883@126.com (Y. Cai), dongqian136@126.com (Q. Dong), xuhaocugb@163.com (H. Xu), hesheng201410@163.com (S. He).

https://doi.org/10.1016/j.apgeochem.2018.11.008
Received 11 July 2018; Received in revised form 10 November 2018; Accepted 13 November 2018
Available online 17 November 2018
0883-2927/ 

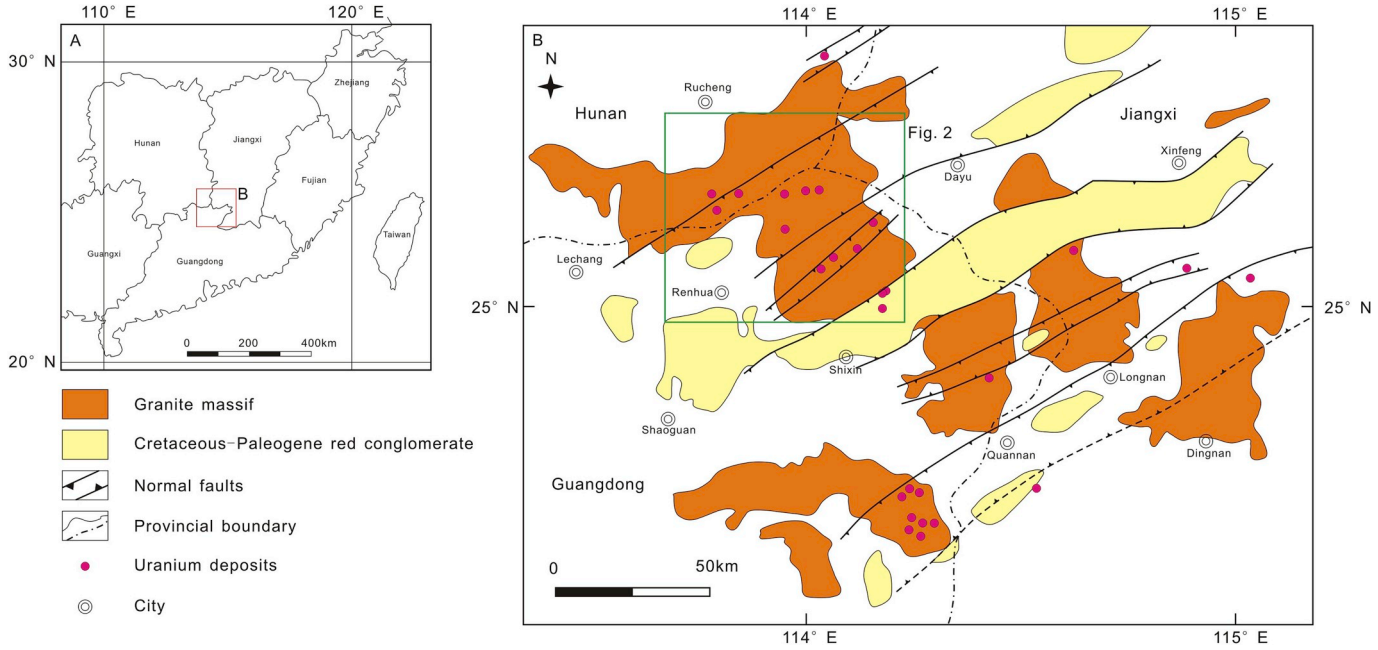


**Fig. 1.** Sketch map showing the approximate location of South Zhuguang uranium ore field (A), and the spatial relationship between uranium deposits, granite massif, major faults, and adjacent Cretaceous-Paleogene basins (B) (Deng et al., 2003b; Hu et al., 2008; Luo et al., 2015).

surface), which make these ore deposits economically viable (Zhang et al., 2017). Since the 1980s, numerous studies have considered the genesis of the South Zhuguang U ore field (e.g., Du and Wang, 1984; Li, 1989; Gong, 1990; Jin and Liu, 1993; Liu and Jin, 1993, 1994; Zhang et al., 2007; Zhang, 2008; Zhang et al., 2017, 2018a). However, the origins of the ore field remain controversial.

Various models have been proposed to explain the formation of granite-related U deposits, including the supergene (e.g., Li, 1990; Li et al., 1995), magmatic–hydrothermal (e.g., Deng et al., 2003a), hot-spot or mantle-derived (e.g., Liu and Jin, 1994; Wang et al., 1999; Zhang et al., 2005), and basin (Zhang et al., 2017, 2018a) models. Combinations of these models have also been proposed (e.g., Hu et al., 2008, 2009; Zhang, 2008; Luo et al., 2015). The diversity of these genetic models is largely due to different interpretations of H, C, O, S, He, and Ar isotopic data (e.g., Li et al., 1995; Wang et al., 1999; Hu et al., 2009), with results from different isotopic systems resulting in conflicting interpretations.

## 2. Geological setting

In South Zhuguang, the geological units can be generally classified into three types according to lithology and age: granite massif, metamorphic basement, and red conglomerates (Zhang et al., 2017, 2018a). The Zhuguang granite massif is the dominant ore-hosting unit, covers an area of > 4000 km$^2$, and has been the focus of most previous studies of the region (e.g., Du et al., 1982; Chen and Jahn, 1998; Chen et al., 1998a; Shu, 2004; Zhang et al., 2005; Sun et al., 2010) (Figs. 1 and 2). This granite massif consists mainly of granodiorite, monzonitic granite, biotite granite, and two-mica granite, all of which have U contents of ~ ppm, locally up to 20 ppm (Zhang, 2008). The massif formed from 416 to 105 Ma, but mainly 244–155 Ma (Shu et al., 2004; Zhang, 2008; Deng et al., 2011), which corresponds to the Indosinian and Yanshanian tectonic events (Faure et al., 2017). In addition to the granite massif, mafic dikes along E–W-striking faults were emplaced in three stages at 139–143, 103–110, and 82–88 Ma (Li et al., 1997; Luo et al., 2015). The dike intrusion events coincide with regional extension that resulted in the formation of Cretaceous–Paleogene redbed basins (Chen et al., 1998b; Hu et al., 2008; Luo et al., 2015).

The Zhuguang granite massif is surrounded by Sinian–Carboniferous marine sedimentary rocks that are 20 km thick (Zhang, 2008). These rocks form the basement of the later redbed basins (Jiangxi BGMR, 1984; Guangdong BGMR, 1988; Hunan BGMR, 1988) and are separated from the latter by a Jurassic–Cretaceous disconformity (Figs. 2 and 1S). The geology of this area comprises three stratigraphic sequences that are separated by disconformities between the Ordovician–Devonian and Permian–Triassic (Fig. 1S). The lowest sequence includes Sinian, Cambrian, and Ordovician strata that were originally intercalated sandstone, mudstone, and limestone (Jiangxi BGMR, 1984; Guangdong BGMR, 1988; Hunan BGMR, 1988). This sequence experienced weak metamorphism and was transformed to slate and phyllite, with U contents of 4–10 ppm (Zhang, 2008). The middle sequence comprises Devonian, Carboniferous, and Permian limestone, sandstone, mudstone, and minor coal seams, with U contents of 2–4 ppm (Jiangxi BGMR, 1984; Guangdong BGMR, 1988; Hunan BGMR, 1988). Unlike the lowest sequence, which formed in a shallow marine environment, the middle sequence formed mainly in a deep marine environment (Zhang, 2008). The upper sequence, which is mainly exposed to the south of the Zhuguang granite massif, includes Triassic and Jurassic strata that are typically clastic rocks (i.e., molasse and redbed formations), all of which formed in lacustrine, graben, or intermontane basin settings (Jiangxi BGMR, 1984; Guangdong BGMR, 1988; Hunan BGMR, 1988).

The Cretaceous–Paleogene redbeds, which comprise dominantly conglomerate and sandstone, were formed in graben or intermontane basin environments (Wan, 2004). The basin infill was sourced mainly from the surrounding granite massif and basement, and also contains a minor biodetrital component. The U content of the basin infill is generally 6–10 ppm, locally up to 15 ppm (CNG, 2005; Zhang, 2008).

In the South Zhuguang area, the most important faults are NE–SW- to NNE–SSW-striking brittle extensional faults that controlled the formation of post-Jurassic redbed basins (Figs. 1 and 2). Most of the U deposits lie close to these faults, suggesting they played an important role in controlling U mineralization (Zhang et al., 2017). In addition, NNW–SSE-striking faults were important because they are the primary ore-hosting structures and typically contain vein- or breccia-type ores. The E–W-striking faults are usually the dike-hosting structures (CNG and BRIUG, 2010).

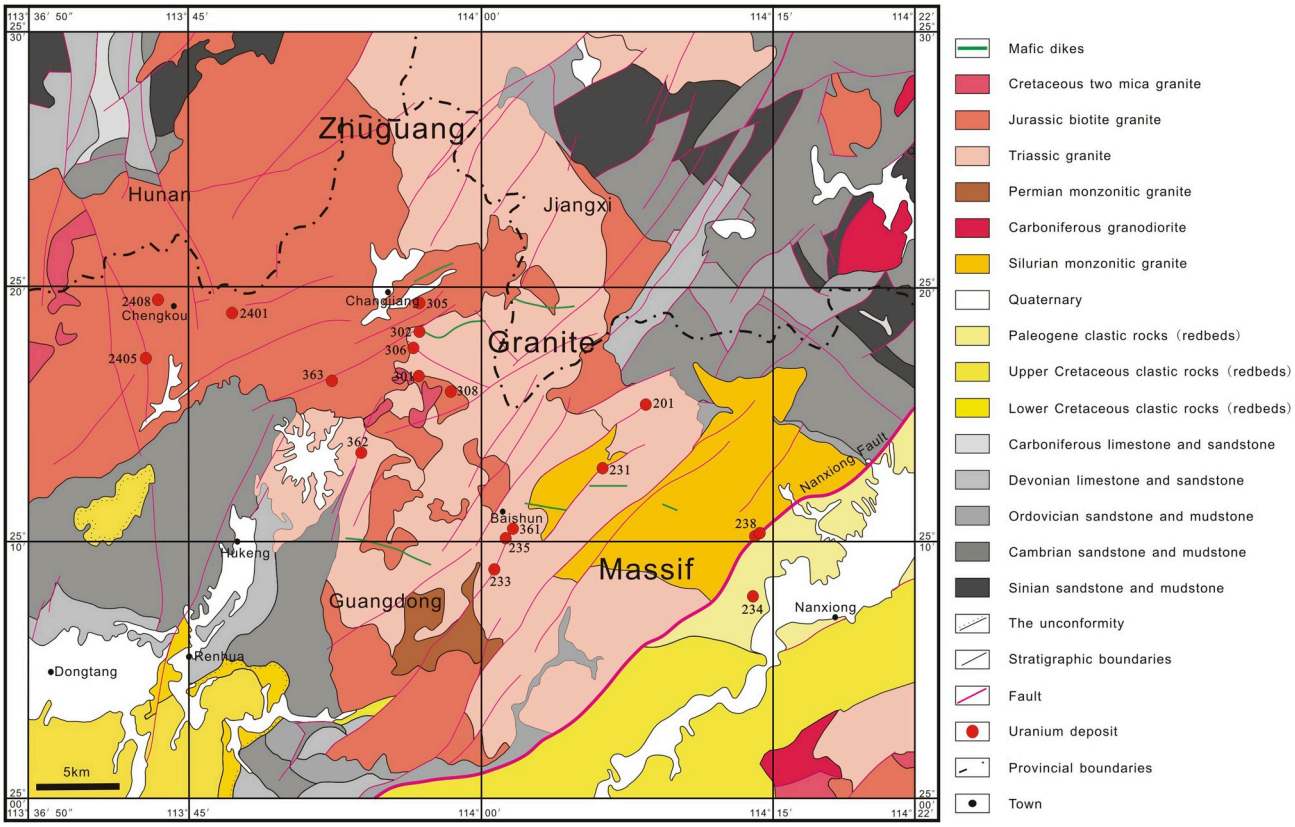


**Fig. 2.** Simplified geological map for South Zhuguang uranium ore field, showing the distribution of uranium deposits, granite massif, metamorphic basement, and redbed basins (Hu et al., 2008; Zhang, 2008).

## 3. Ore deposit geology

There are ~20 U deposits in the South Zhuguang area, which from west to east are named the 2408, 2405, 2401, 363, 305, 302, 306, 301, 308, 362, 201, 231, 361, 235, 233, 238, and 234 deposits (Fig. 2). The deposits comprise predominantly vein-shaped ore bodies in the granite massif, although a small number of deposits are hosted in adjacent Cretaceous–Paleogene redbed basins (Figs. 1 and 2S). A detailed description of these deposits has been given by Zhang et al. (2017, 2018a) and Dahlkamp (2009), and so they are only briefly described here. The vein-type ore bodies are found in silicified, high-angle normal faults, are generally 50–1000 m in length along strike, and tens of meters wide. Typically, the major ore bodies have vein, breccia, or stockwork textures, with a relatively high-grade core surrounded by lower-grade mineralization (Zhang et al., 2017, 2018a).

Typical ores consist of pitchblende, hematite, quartz, fluorite, calcite, and locally pyrite (Fig. 3S). The pitchblende is usually present in fractures and was deposited in multiple substages, as indicated by the intergrown hematite and uraninite (Fig. 3S A, B, and E) and associated pyrite (Fig. 3S B, C, and F). The quartz, fluorite, calcite, and hematite in the veins can be divided into three associations. The first includes quartz and fluorite (Fig. 4S A), both of which are associated with pitchblende and pyrite. The second is superimposed on the first (Fig. 3S B), and generally comprises pitchblende, quartz, calcite, and occasional pyrite (Fig. 4S B). The third formed during the post-ore stage (Fig. 4S C). The types of hydrothermal alteration in the South Zhuguang U ore field have been described in previous studies (i.e., Li, 1990; Li et al., 1996; Zhang, 2008; Gao et al., 2011a, b) that divided the alteration into pre-, syn-, and post-ore stages. The pre-ore alteration is predominantly albitization that developed extensively in the ore-hosting granites (Zhang et al., 2018b). The syn-ore types of alteration include silicification, hydromicazation, hematization, and chloritization that developed adjacent to ore-bearing faults, and outwards for hundreds of meters into the unaltered granites (Zhang et al., 2018a). The post-ore alteration was typically hematization, fluoritization, and carbonatation that occurred along fractures and veins (Zhang et al., 2018b). In summary, these three stages include a pre-ore magmatic stage that formed the rocks that were later affected by hydrothermal alteration, syn-ore hydrothermal stages that formed quartz–pitchblende–fluorite (stage 1) and quartz–pitchblende–calcite (stage 2), and a post-ore stage that formed quartz, hematite, fluorite, and calcite (Fig. 4S).

## 4. Genesis of granite-related uranium mineralization: a review

Du et al. (1982) proposed the supergene model, whereby U is derived from uraniferous granites (Li, 1990; Li et al., 1995; Zhang, 2008) and fracture zones provide the pathways and sites for post-magmatic hydrothermal processes involving meteoric waters, resulting in the formation of ore-bearing veins.

Given that the ore-hosting rocks are predominantly granites, some studies have proposed that the ore-forming fluid is dominantly magmatic water (i.e., the (residual) magmatic–hydrothermal model), possibly contaminated by meteoric water. This fluid then extracts U from the granites and deposits it along fractures (Zhou, 1996; Min et al., 1999, 2005; Deng et al., 2003a, b; Zhou et al., 2003). Zhou (1996) proposed a model that involves at least two stages of U mineralization. In the first stage, the ore-forming fluid is a residual, uraniferous magmatic fluid. The second stage involves mainly supergene processes, whereby meteoric waters extract U from uraniferous granites and then migrate and deposit pitchblende in fault zones (i.e., the supergene model). Min et al. (1999) proposed a more detailed genetic model that combined the (residual) magmatic–hydrothermal and supergene models. During magma intrusion, magmatic fluids separate from an oversaturated magma, resulting in the chloritization, argillization, and

damouritization of ore-hosting granites, which facilitates leaching of U by later, deeply circulating meteoric waters. Uranium deposition is then probably triggered by $CO_2$ loss from the ore-forming fluid due to fluid–rock interaction.

Li (2006) suggested that granite-related U deposits were genetically related to a mantle plume (i.e., a hot-spot or mantle-derived model) that was active from 220 to 50 Ma in southern China. The long duration of magmatism resulted in numerous granitic intrusions and mafic dikes, enriched the crust in U, and ultimately led to U mineralization.

Hu et al. (2008) proposed that Cretaceous–Tertiary crustal extension in South China, associated with the intrusion of abundant mafic dikes, resulted in the upward migration of mantle-derived $CO_2$ that reacted with meteoric water to form $CO_2$-rich hydrothermal fluids (Hu et al., 1993). Heat from the mafic magmas drove the circulation of $CO_2$-rich hydrothermal fluids within fault systems in U-bearing source rocks (surrounding volcanic rocks, granites, and black shales) and remobilized the U as soluble $UO_2(CO_3)_2^{2-}$ and $UO_2(CO_3)_3^{4-}$. Subsequently, pressure release and $CO_2$ degassing resulted in the dissociation of the uranyl carbonate complexes, which is a key factor in the formation of many U deposits.

Luo et al. (2015) reported in situ U–Pb uraninite ages for the Xianshi deposit (Taoshan–Zhuguang belt) of 135, 113, and 104 Ma, all of which coincide with the ages of three generations of mantle-derived mafic dikes. Consequently, the authors suggested that the Xianshi deposit had experienced at least three hydrothermal events responsible for U mineralization, which were genetically related to the emplacement of these mafic dikes (i.e., the mantle-derived model).

Based on a comparison of U-bearing and barren granites in southern China, Zhao et al. (2011, 2016) proposed that U mineralization was genetically related to reduced and strongly peraluminous granites, and was derived from U-rich pelitic rocks. Zhang et al. (2017, 2018a) suggested a genetic model similar to that proposed for unconformity-related deposits (i.e., a basinal model; Kyser et al., 2000; Cuney et al., 2003; Cuney and Kyser, 2008), based on a detailed investigation of fluid inclusions and hydrothermal alteration, and H–O isotopic data. In this model, the ore-forming fluids were derived initially from meteoric water, and became U- and $CO_2$-bearing fluids through water–sediment interactions in the Cretaceous–Paleogene basin, which made them similar to basinal fluids in terms of their H–O isotopic compositions. The U-bearing fluids then flowed into the Zhuguang granite massif through regional faults. When the ore-forming fluids entered faults, they reacted with the granites adjacent to the faults, and this would have reduced the oxidation state, converted $U^{6+}$ to $U^{4+}$, and produced a decrease in the saturation solubility of U. In addition to this alteration, $CO_2$ degassing or phase separation led to the release of $CO_2$ and the decomposition of uranyl carbonate complexes ($UO_2(CO_3)_2$), thereby promoting U deposition.

Granite-related ore bodies are generally found in fracture zones that crosscut the granites, which suggests that the U mineralization is much younger than the granites (Zhou et al., 2003; CNG, 2005; Dahlkamp, 2009; Wang et al., 2014). This also means that little magmatic fluid would have remained during U mineralization, and the ore-forming fluid would therefore have been amagmatic. The occurrence of U ore bodies in Paleogene basins indicates the mineralization in the South Zhuguang area is no older than 65 Ma (Fig. 2S D). Using a U–Pb isochron age of pitchblende, previous studies have suggested the mineralization in the South Zhuguang area occurred at 70–56 Ma, which coincides with the formation of the Cretaceous–Paleogene redbed basins in the south (Zhang, 2008; Huang et al., 2010). In addition, U–Pb dating of pitchblende by Zhang et al. (2018a) produced three isochron ages that correspond to the syn- and post-ore stages. The syn-ore stages I and II occurred at ca. 57 and 53 Ma, respectively, and the post-ore stage at ca. 49 Ma (Zhang et al., 2018a).

Previous studies have argued that the ore-forming fluid was initially meteoric water, which extracted U from altered granites. However, this is inconsistent with the fact that the altered granites are typically richer in U than the unaltered granites, indicating that alteration is generally a U addition process (CNG and BRIUG, 2010; Zhang et al., 2017). With regards to the hot-spot or mantle-derived model, the extremely low mantle U content and low U solubility in reducing fluids (Robb, 2005) appear to rule this out as a viable genetic model. Moreover, mafic–ultramafic magmatism in the South Zhuguang area is tens of millions of years older than the U mineralization, meaning that it could not have been responsible for the pervasive U mineralization in this region.

The differences in the previously described genetic models are due mainly to varied interpretations of stable isotope data. For example, Zhang et al. (2017) suggested the ore-forming fluid was sourced from the redbed basins, based on H–O isotopic data. However, Zhang et al. (2008) proposed that mantle-derived $CO_2$ had an important role in the ore-forming process, although the authors did not consider the effects of various geological processes on stable isotopic data. In the present study, we propose a new model for U mineralization that is consistent with the multiple stable isotopic systems.

**Table 1**
Ion and gas compositions of fluid inclusions in different stages and minerals.

| Deposit | Sample No. | Stage | Mineral | Ion composition in liquid phase (μg/g) | | | | | | | | Gas composition (μl/g) | | | | | |
|---|---|---|---|---|---|---|---|---|---|---|---|---|---|---|---|---|---|
| | | | | $F^-$ | $Cl^-$ | $NO_3^-$ | $SO_4^{2-}$ | $Na^+$ | $K^+$ | $Mg^{2+}$ | $Ca^{2+}$ | $H_2$ | $N_2$ | CO | $CH_4$ | $CO_2$ | $H_2O$ |
| 302 | P29 | I | Quartz | 5.539 | 0.319 | 0.187 | 223.1 | 2.770 | 3.279 | 1.2800 | 44.91 | 0.0981 | 0.4753 | 0.0656 | 0.0547 | 1.333 | $1.960 \times 10^5$ |
| 302 | P31 | I | Quartz | 4.602 | 0.198 | 0.163 | 147.4 | 2.107 | 2.605 | 1.0572 | 30.78 | 0.2357 | 0.5523 | 0.1271 | 0.0172 | 1.414 | $1.352 \times 10^5$ |
| 301 | 027–3 | I | Quartz | 3.932 | 0.278 | 0.168 | 206.3 | 1.921 | 1.392 | 1.9476 | 19.74 | 0.0379 | 0.3118 | 0.0943 | 0.0937 | 1.043 | $3.131 \times 10^5$ |
| 302 | P35 | I | Quartz | 4.228 | 0.267 | 0.120 | 112.5 | 2.743 | 2.037 | 1.0208 | 20.82 | 0.2918 | 0.7412 | 0.1025 | 0.0551 | 1.171 | $2.110 \times 10^5$ |
| 301 | 025–1 | I | Fluorite | 9.224 | 0.174 | 0.176 | 41.6 | 1.091 | 2.404 | 0.2011 | 26.56 | 0.4436 | 0.1667 | 0.1924 | 0.0541 | 1.037 | $1.381 \times 10^5$ |
| 301 | 025–2 | I | Fluorite | 12.116 | 0.408 | 0.160 | 90.7 | 2.914 | 2.511 | 0.3998 | 20.36 | 0.0524 | 0.4716 | 0.1338 | 0.0383 | 1.088 | $1.582 \times 10^5$ |
| 302 | ZK2-2-1 | II | Quartz | 0.460 | 0.860 | 2.487 | 99.2 | 10.690 | 9.873 | 0.4115 | 27.38 | 0.4005 | 0.2711 | 0.1984 | 0.1001 | 2.350 | $6.708 \times 10^5$ |
| 302 | P30 | II | Quartz | 0.623 | 0.715 | 2.093 | 107.2 | 17.800 | 6.201 | 0.4831 | 74.14 | 0.4726 | 0.1414 | 0.0927 | 0.1273 | 2.139 | $4.693 \times 10^5$ |
| 302 | P33 | II | Quartz | 0.713 | 0.814 | 1.885 | 71.9 | 6.810 | 7.346 | 0.3166 | 30.22 | 0.2473 | 0.3402 | 0.0316 | 0.1926 | 2.750 | $2.329 \times 10^5$ |
| 302 | ZK4-2-3 | II | Calcite | 0.383 | 0.730 | 0.350 | 105.9 | 8.250 | 0.515 | 0.6269 | 89.73 | 0.3863 | 0.2623 | 0.1252 | 0.0836 | 0.956 | $3.516 \times 10^5$ |
| 302 | P27 | II | Calcite | 0.216 | 1.014 | 0.828 | 84.4 | 11.920 | 0.316 | 0.5327 | 104.25 | 0.4155 | 0.2043 | 0.0817 | 0.1082 | 0.779 | $1.284 \times 10^5$ |
| 302 | P32 | II | Calcite | 0.069 | 0.648 | 0.343 | 144.4 | 13.280 | 0.729 | 0.5739 | 85.48 | 0.4835 | 0.2190 | 0.1759 | 0.1884 | 0.961 | $1.521 \times 10^5$ |
| 301 | −10006 | II | Calcite | 0.333 | 0.553 | 0.287 | 122.3 | 1.023 | 0.256 | 0.5580 | 70.13 | 0.1536 | 0.3761 | 0.0441 | 0.0140 | 0.738 | $1.634 \times 10^5$ |

$Br^-$, $NH_4^+$, $Li^+$, $Cs^+$, $Sr_2^+$, $Ar_2$, $O_2$ and $C_nH_m$ ($n \geq 2$; $m \geq 4$) are below detection limit.
$HCO_3^-$ and $CO_3^{2-}$ contents were not measured with using ion chromatographic analytical methods separately.

## 5. Samples and analysis

Samples of ores, altered and unaltered granites, and fluorite veins were mostly collected from drilling cores and tunnels in the 301, 302, 305, 306, and 308 deposits of the South Zhuguang U ore field (Table 1S). Polished thin-sections were prepared from all samples and examined under transmitted and reflected light to determine the mineral paragenesis and contents of secondary fluid inclusions, using a polarizing microscope (DM2500P, LEICA Microsystems) at the Laboratory of Rock and Mineral Identification, Division of Geology and Mineral Resources, Beijing Research Institute of Uranium Geology, Beijing, China. Only the samples in which secondary fluid inclusions are relatively rare (≤5%) were selected for subsequent analyses.

After petrographic examination of each sample, the host rock material was removed, and pitchblende ± quartz ± calcite ± fluorite ± pyrite veins were washed with distilled water, dried naturally, and crushed into fine grains for later mineral separation. Quartz, calcite, pyrite, and fluorite grains were handpicked under a binocular stereo-microscope to obtain representative fractions weighing ≥1 g for chemical and isotopic analyses.

The types of fluid inclusions in the quartz, calcite, and fluorite from the syn- and post-ore veins, as well as microthermometry data and laser Raman analyses, have already been described in detail (Zhang, 2008; Zhang et al., 2017), and thus are only briefly descried here. Bulk volatile and ionic compositions of fluid inclusions were analyzed by combined gas and ion chromatography (Bray et al., 1991; Channer et al., 1999) using PE.Clarus600 and DIONEX-500 gas and ion chromatography systems, respectively, at the Geological Analysis and Testing Center, Beijing Research Institute of Uranium Geology. Analyses were conducted on seven quartz, four calcite, and two fluorite samples from the 301 and 302 deposits (sample mass ~2 g). $Br^-$, $NH_4^+$, $Li^+$, $Cs^+$, $Sr^{2+}$, $Ar_2$, $O_2$, and $C_nH_m$ (n ≥ 2; m ≥ 4) were all below detection limits, and $HCO_3^-$ and $CO_3^{2-}$ contents were not separately measured with the ion chromatographic analytical methods.

In addition to the isotopic data presented by Hu (1984), Li et al. (1995), Huang (1996), Zhang (2008), and Zhang et al. (2017), we obtained further data for a series of samples that were collected from different deposits: (1) 15 pitchblende–quartz veins were analyzed for the O–H isotopic composition of quartz and quartz-hosted fluid inclusions (5 and 10 samples from the 308 and 305 deposits, respectively); (2) 28 altered and unaltered granites were analyzed for their whole-rock O isotopic compositions (8, 9, and 11 samples from the 306, 301, and 302 deposits, respectively); (3) 6 pitchblende–calcite vein samples from the 302 deposit were analyzed for the C–O isotopic composition of calcite; (4) 17 pyrite-rich ore samples were analyzed for the S isotopic composition of pyrite (4 and 13 samples from the 306 and 302 deposits, respectively); and (5) 5 pitchblende–fluorite and 4 pure fluorite vein samples from the 302 deposit were analyzed for the Sr isotopic composition of fluorite.

Oxygen isotopic compositions of quartz, and altered and unaltered granite were measured using the $BrF_5$ method of Clayton and Mayeda (1963). The results are reported relative to VSMOW, and the analytical precision and accuracy are both ± 0.2‰, as assessed by analysis of Chinese national quartz standards GBW-04409 ($\delta^{18}O$ = 11.11‰ ± 0.06‰) and GBW-04409 ($\delta^{18}O$ = −1.75‰ ± 0.08‰). Hydrogen isotopic compositions of quartz-hosted fluid inclusions were determined using the methods of Kyser and O'Neil (1984). The results are reported in δ notation in units of per mil (‰) relative to VSMOW. Replicate δD analyses were reproducible to ± 1‰. Two standards were analyzed throughout the course of this study: Peking University ($\delta D_{V\text{-}SMOW}$ = −64.8‰) and Lanzhou ($\delta D_{V\text{-}SMOW}$ = −84.55‰).

Oxygen and C isotopic compositions of calcite were measured using the method of Mccrea (1950). The results are reported in δ notation in units of per mil (‰) relative to the VPDB standard. Replicate $\delta^{13}C_{V\text{-}PDB}$ and $\delta^{18}O_{V\text{-}PDB}$ values were reproducible to ± 0.1‰ and ± 0.2‰, respectively. Two Chinese national rock standards were analyzed throughout the course of this study: GB04416 ($\delta^{13}C_{V\text{-}PDB}$ = 1.61‰ ± 0.03‰; $\delta^{18}O_{V\text{-}PDB}$ = −11.59‰ ± 0.11‰) and GB04417 ($\delta^{13}C_{V\text{-}PDB}$ = −6.06‰ ± 0.06‰; $\delta^{18}O_{V\text{-}PDB}$ = −24.12‰ ± 0.19‰). All the O, H, and C isotopic analyses were performed using a Finnigan MAT 253 mass spectrometer.

Sulfur isotopic compositions of pyrite were measured using the methods of Robinson and Kusakabe (1975) and a Finnigan MAT 251 mass spectrometer. The results are reported in δ notation in units of per mil (‰) relative to the CDT standard. Replicate $\delta^{34}S_{V\text{-}CDT}$ values were reproducible to ± 0.2‰. Two Chinese national standards were analyzed throughout the course of this study: GB04414 ($\delta^{34}S_{V\text{-}CDT}$ = −0.07‰ ± 0.13‰) and GB04415 ($\delta^{34}S_{V\text{-}CDT}$ = 22.15‰ ± 0.14‰).

Rubidium and Sr isotopic compositions of fluorite were measured using the methods of Nakamura et al. (1976) and an ISOPROBE-T mass spectrometer. Estimated uncertainties at the 2 sigma level are ± 1% for the $^{87}Rb/^{86}Sr$ concentration ratio and ± 0.02% for the $^{87}Sr/^{86}Sr$ ratio. Analysis of the NBS987 standard from the US National Institute for Standards and Testing (NIST) yielded $^{87}Sr/^{86}Sr$ = 0.710250 ± 7. The Rb–Sr isotopic analyses were performed at the Geological Analysis and Testing Center, Beijing Research Institute of Uranium Geology.

## 6. Results and interpretations

### 6.1. Bulk volatile and ionic compositions of fluid inclusions

The results of the gas and ion chromatographic analyses are summarized in Tables 1 and 2. The volatile components are generally

**Table 2**
Comparison of $F^-/Cl^-$, $\Sigma(F^- + Cl^- + NO_3^- + 2SO_4^{2-})$, $\Sigma(Na^+ + K^+ + 2Mg^{2+} + 2Ca^{2+})$, $H_2/N_2$, and $CO_2/CH_4$ ratios between Stage I and II.

| Deposit | Sample No. | Stage | Mineral | $F^-/Cl^-$ | $\Sigma(F^- + Cl^- + NO_3^- + 2SO_4^{2-})$ (μmol/g) | $\Sigma(Na^+ + K^+ + 2Mg^{2+} + 2Ca^{2+})$ (μmol/g) | $H_2/N_2$ | $CO_2/CH_4$ |
|---|---|---|---|---|---|---|---|---|
| 302 | P29 | I | Quartz | 32.407 | 4.951 | 2.555 | 2.890 | 8.862 |
| 302 | P31 | I | Quartz | 43.365 | 3.321 | 1.784 | 5.975 | 29.894 |
| 301 | 027–3 | I | Quartz | 26.390 | 4.515 | 1.267 | 1.702 | 4.048 |
| 302 | P35 | I | Quartz | 29.501 | 2.576 | 1.297 | 5.512 | 7.728 |
| 301 | 025–1 | I | Fluorite | 98.681 | 1.361 | 1.454 | 37.255 | 6.970 |
| 301 | 025–2 | I | Fluorite | 55.393 | 2.541 | 1.242 | 1.556 | 10.330 |
| 302 | ZK2-2-1 | II | Quartz | 0.999 | 2.155 | 2.121 | 20.682 | 8.537 |
| 302 | P30 | II | Quartz | 1.625 | 2.321 | 4.680 | 46.792 | 6.110 |
| 302 | P33 | II | Quartz | 1.634 | 1.588 | 2.022 | 10.177 | 5.192 |
| 302 | ZK4-2-3 | II | Calcite | 0.979 | 2.253 | 4.910 | 20.618 | 4.158 |
| 302 | P27 | II | Calcite | 0.397 | 1.811 | 5.783 | 28.473 | 2.618 |
| 302 | P32 | II | Calcite | 0.200 | 3.035 | 4.917 | 30.909 | 1.855 |
| 301 | −10006 | II | Calcite | 1.125 | 2.586 | 3.603 | 5.718 | 19.169 |

present in the following order of abundance: $H_2O$ > $CO_2$ > $N_2$ > $H_2$ > CO > $CH_4$. However, in a few cases, $H_2$ was slighter less abundant than CO and $CH_4$. Water is the predominant volatile species. $CO_2$ contents vary from 1.043 to 1.414 μL/g for quartz-hosted fluid inclusions and 1.037–1.088 μL/g for fluorite-hosted fluid inclusions from syn-ore stage I. $CO_2$ contents vary from 2.139 to 2.750 μL/g for quartz-hosted fluid inclusions and 0.738–0.961 μL/g for calcite-hosted fluid inclusions from syn-ore stage II. $N_2$, $H_2$, and $CH_4$ contents are 0.3118–0.7412, 0.0379–0.2918, and 0.0172–0.0937 μL/g, respectively, for stage I quartz-hosted fluid inclusions; 0.1667–0.4716, 0.0524–0.4436, and 0.0383–0.0541 μL/g, respectively, for stage I fluorite-hosted fluid inclusions; 0.1414–0.3402, 0.2437–0.4726, and 0.1001–0.1926, respectively, for stage II quartz-hosted fluid inclusions; and 0.2043–0.3761, 0.1535–0.4835, and 0.0140–0.1884, respectively, for stage II calcite-hosted fluid inclusions.

Using ion chromatographic analysis of liquids from the same samples (Bray et al., 1991; Channer et al., 1999), $Ca^{2+}$ and $SO_4^{2-}$ were determined to be the principal ions in all samples (Table 1). In addition, smaller amounts of $F^-$, $Cl^-$, $NO_3^-$, $Na^+$, $K^+$, and $Mg^{2+}$ were detected in all samples. All other ions were below detection limits, or their blanks values were > 25% of those in the sample leachates.

The previous determination of the types of fluid inclusions in quartz, calcite, and fluorite from syn- and post-ore veins in this study, as well as microthermometry data and laser Raman analyses (Zhang, 2008; Zhang et al., 2017), enable a robust interpretation of the bulk volatile and ionic compositions of the fluid inclusions. The fluid trapped in the syn-ore stage is probably $CaSO_4$-dominated, low to intermediate salinity (Zhang, 2008; Zhang et al., 2017), and $CO_2$-rich. However, the bulk volatile and ionic compositions of fluid inclusions from the different stages are variable (Tables 1 and 2). The $F^-/Cl^-$ ratios are 26.4–98.7 for syn-ore stage I and 0.20–1.63 for syn-ore stage II. The $\Sigma(F^- + Cl^- + NO_3^- + 2SO_4^{2-})$ values are 1.36–4.95 μg/g and 1.59–3.04 μg/g for syn-ore stages I and II, respectively, and $\Sigma(Na^+ + K^+ + 2Mg^{2+} + 2Ca^{2+})$ values are 1.24–2.56 μg/g and 2.02–5.78 μg/g for syn-ore stages I and II, respectively. $H_2/N_2$ ratios for syn-ore stage I are generally < 6 (1.56–5.98), with one anomalous value of 37.255, whereas for syn-ore stage II the values are generally > 10 (10.18–46.79), with the exception of one anomalous value of 5.72. $CO_2/CH_4$ ratios are 4.05–29.89 and 1.86–19.17 for syn-ore stages I and II, respectively (Table 2; Fig. 3).

The high $F^-$ contents of syn-ore stage I provide insights into the formation of fluorite, whereas the low $F^-$ contents of syn-ore stage II correspond to higher contents of $Ca^{2+}$, due to the following reaction:

$$Ca^{2+} + 2F^- = CaF_2 (\downarrow)$$

The fluid trapped in quartz veins of the syn-ore stage has variable $CO_2/CH_4$ ratios (Fig. 3), and the range of stage II is smaller than that of stage I. $CO_2$ is the major non-$H_2O$ volatile component in all fluid inclusions. As suggested by Zhang et al. (2017) and Zhang (2008), the ore-forming fluid of the syn-ore stages experienced $CO_2$ degassing (phase separation), which probably resulted in the wide range of $CO_2/CH_4$ ratios. $H_2/N_2$ ratios of the fluid in syn-ore stage I are generally constant, but were more variable during stage II. The $N_2$ contents of the ore-forming fluid were generally constant (Table 2), whereas the $H_2$ content in syn-ore stage II was much higher than that in syn-ore stage I, which indicates that the ore-forming fluid became more reduced over time (Zhang et al., 2017).

The ore-forming fluids mainly contained eight types of ions. A plot of $\Sigma(F^- + Cl^- + NO_3^- + 2SO_4^{2-})$ vs. $\Sigma(Na^+ + K^+ + 2Mg^{2+} + 2Ca^{2+})$ shows that the total anion valence is generally higher than that of cations for syn-ore stage I, but is lower for stage II (Fig. 3). $HCO_3^-$ and $CO_3^{2-}$ contents were not measured by ion chromatography. For syn-ore stage I, there are two possibilities regarding the $HCO_3^-$ and $CO_3^{2-}$ contents: (1) little $HCO_3^-$ and $CO_3^{2-}$ were present, meaning that $H^+$ supplemented the cation shortage and the ore-forming fluid was acidic; or (2) there was some $HCO_3^-$ and $CO_3^{2-}$ present, meaning that the total anion valence was higher than that determined. In the latter possibility, even more $H^+$ is necessary to

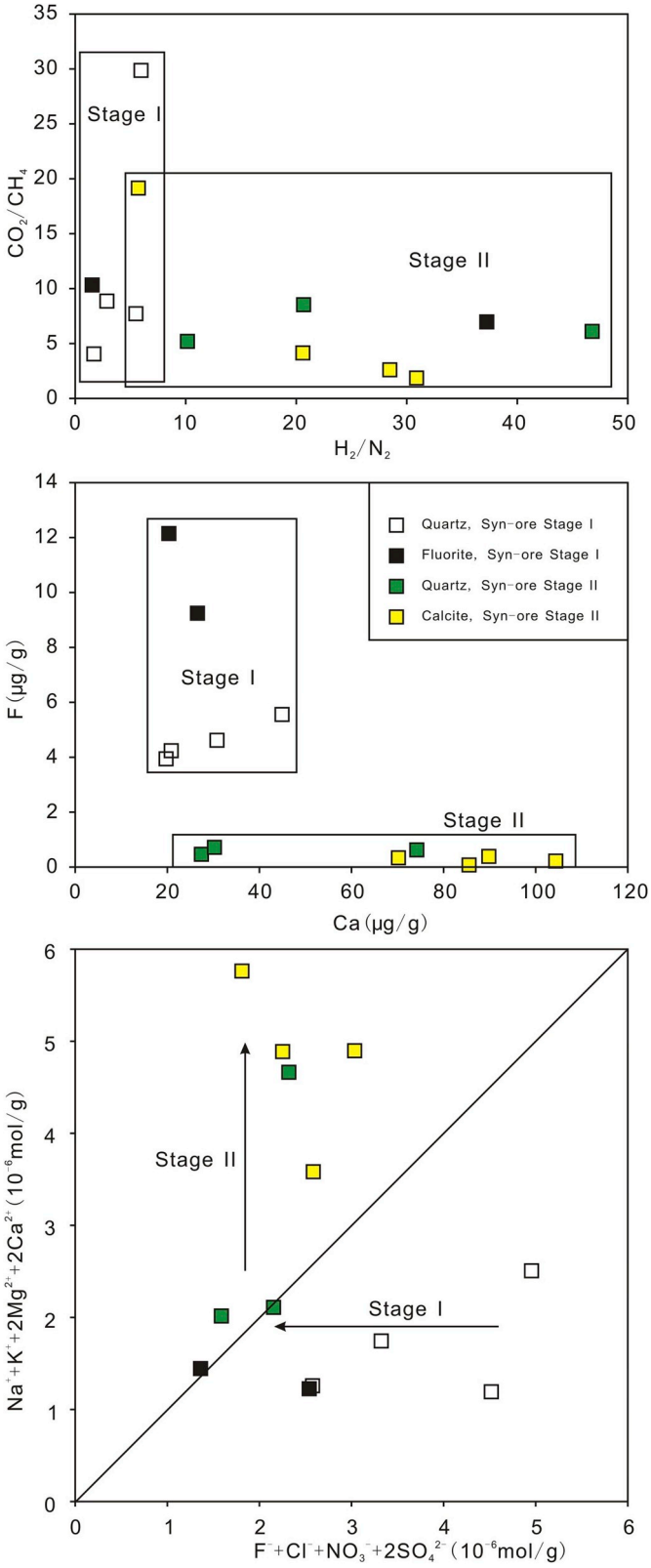


**Fig. 3.** Plots of $CO_2/CH_4$ vs $H_2/N_2$, $F^-$ vs $Ca^{2+}$, and $\Sigma(F^- + Cl^- + NO_3^- + 2SO_4^{2-})$ vs $\Sigma(Na^+ + K^+ + 2Mg^{2+} + 2Ca^{2+})$, all of which showing the difference of ore-forming fluid between syn-ore stage I and II.

balance the valence difference. However, in this situation the $HCO_3^-$ and $CO_3^{2-}$ would react with $H^+$ to form $H_2O$ and $CO_2$, respectively. In summary, during syn-ore stage I there was little to no $HCO_3^-$ or $CO_3^{2-}$ in the ore-forming fluid, and the fluid was acidic.

For syn-ore stage II, there are three possibilities regarding the $HCO_3^-$ and $CO_3^{2-}$ contents: (1) the $HCO_3^-$ and $CO_3^{2-}$ contents are not sufficient to balance the valence difference between $\Sigma(F^- + Cl^- + NO_3^- + 2SO_4^{2-})$ and $\Sigma(Na^+ + K^+ + 2Mg^{2+} + 2Ca^{2+})$ (Fig. 3), which means there must have been $OH^-$ present to supplement the shortage of anions, and the ore-forming fluid was alkaline; (2) the $HCO_3^-$ and $CO_3^{2-}$ contents were high enough to precisely balance the valence difference between $\Sigma(F^- + Cl^- + NO_3^- + 2SO_4^{2-})$ and $\Sigma(Na^+ + K^+ + 2Mg^{2+} + 2Ca^{2+})$ (Fig. 3), which means the ore-forming fluid was alkaline, because $HCO_3^-$ and $CO_3^{2-}$ form weak acids; or (3) $\Sigma(HCO_3^- + 2CO_3^{2-} + F^- + Cl^- + NO_3^- + 2SO_4^{2-}) > \Sigma(Na^+ + K^+ + 2Mg^{2+} + 2Ca^{2+})$, which means that $H^+$ supplemented the shortage of cations and the ore-forming fluid was acidic. However, in this latter possibility, the $H^+$ would have reacted with $HCO_3^-$ and $CO_3^{2-}$ to form $H_2O$ and $CO_2$, respectively, until $H^+$ was almost exhausted, which indicates that $\Sigma(HCO_3^- + 2CO_3^{2-} + F^- + Cl^- + NO_3^- + 2SO_4^{2-})$ cannot have been greater than $\Sigma(Na^+ + K^+ + 2Mg^{2+} + 2Ca^{2+})$. As such, during syn-ore stage II the ore-forming fluid was alkaline.

### 6.2. Oxygen and hydrogen isotopic data for syn-ore quartz

The $\delta^{18}O_{V\text{-}SMOW}$ values vary from +7.3‰ to +12.1‰ and +7.4‰ to +12.8‰ for quartz in the syn-ore stage I and II veins, respectively. $\delta D_{W\text{-}SMOW}$ values of $H_2O$ in fluid inclusions from quartz of syn-ore stages I and II range from −53.4‰ to −97.8‰ and −48.6‰ to −94.3‰, respectively (Table 1S). These O–H isotopic ranges are similar in each syn-ore stage. In combination with previously reported data, $\delta^{18}O_{V\text{-}SMOW}$ values are generally in the range of +6.29‰ to +14.3‰ for quartz in syn-ore stage veins (Table 1S). The $\delta^{18}O_{W\text{-}SMOW}$ values of water in equilibrium with quartz were calculated using the fractionation equation of Clayton et al. (1972) and the average entrapment temperature during U mineralization of 250 °C from Zhang et al. (2017). The calculated water $\delta^{18}O_{W\text{-}SMOW}$ values range from −1.85‰ to +5.35‰. $\delta D_{W\text{-}SMOW}$ values of water in fluid inclusions from quartz of the syn-ore stages range from −104.4‰ to −23.1‰. The O–H isotopic data from the pre- and post-ore stages are from Zhang (2008). The $\delta^{18}O_{V\text{-}SMOW}$, $\delta^{18}O_{W\text{-}SMOW}$, and $\delta D_{W\text{-}SMOW}$ values for the pre-ore stage are +11.4‰ to +12.0‰, +1.67‰ to +4.34‰, and −81.0‰ to −74.0‰, respectively, and those for the post-ore stage are +6.6‰ to +13.3‰, −9.4‰ to +2.4‰, and −99.0‰ to −74.0‰, respectively (Table 1S).

The data of Zhang (2008) (302 deposit), Zhang et al. (2017) (306, 301, and 302 deposits), and Li et al. (1995) (201 deposit) are plotted in Fig. 4, along with our new data. Similar O–H isotopic compositions are evident for the different mineralization stages from the South Zhuguang U deposits, apart from some post-ore data from the 302 deposit. The O isotopic compositions of syn-ore fluids in equilibrium with quartz fall mainly between the values typical of meteoric water and primary magmatic and metamorphic waters, but closer to the latter (Fig. 4). Hydrogen isotopic compositions of syn-ore fluids vary widely across the range of primary magmatic and metamorphic waters, but are slightly higher than values for meteoric water, although within the range of meteoric waters in South China during the Cretaceous to Paleogene (Zhang et al., 1995).

The O–H isotope plots of Zhang (2008) for post-ore fluids show that the data are concentrated in the lower-left field for primary magmatic water, close to the center of the syn-ore O–H isotopic data (Fig. 4). The O–H isotopic compositions of post-ore fluids plot much closer to data for meteoric waters of South China during the Cretaceous to Paleogene, and form a general linear trend (A in Fig. 4). These data generally plot in the basinal fluid field and are parallel to the extension of H–O isotopic data from Alberta, Michigan Basin, and Gulf Coast. This indicates that the post-ore fluid was derived from the Cretaceous–Neogene basins, despite the wide range of isotopic values. The post-ore fluid had a local meteoric origin in general (Clayton et al., 1966; Taylor, 1974), which is consistent with the data plotting close to the meteoric water line. Continental redbeds generally form in arid environments, and the strong evaporation results in the residual water becoming enriched in $^{18}O$ and D (Craig and Gordon, 1965; Sofer and Gat, 1975), which may explain the displacement of δD and $\delta^{18}O$ values away from the meteoric water line toward the field of metamorphic waters. Other isotopic fractionation processes might also have occurred, including isotopic exchange with $^{18}O$-rich sedimentary minerals and D enrichment due to membrane filtration, as well as exchange with $H_2S$, hydrocarbons, and hydrous minerals (Hoefs, 1997).

There is no obvious correlation between the O and H isotopic compositions of syn-ore water. The $\delta^{18}O$ data are concentrated mainly between −1.85‰ and +3.89‰, whereas the δD data have a wide range of values. Given that all the $\delta D_{W\text{-}SMOW}$ values were measured on fluid inclusions in quartz, the differences in $\delta D_{W\text{-}SMOW}$ values cannot be an artifact of different $T_h$ values (Hoefs, 1997; Graupner et al., 2001). In the South Zhuguang area, there has been little deformation and magmatism after U mineralization. Moreover, later secondary fractures in quartz from syn-ore veins are not observed, which means the H isotopic compositions are not the result of multiple hydrothermal stages (Zhang et al., 2017, 2018a).

### 6.3. Oxygen isotopic data for altered and unaltered granites

The $\delta^{18}O$ values for altered granites gradually increase from approximately +4‰ close to the ores to approximately +12‰ in nearly unaltered granites (Table 3; Fig. 5) and, as such, the depletion of $^{18}O$ in the altered granites is negative correlated with distance to the ore-bearing faults. This suggests that hydrothermal alteration was responsible for the $^{18}O$ depletion of the altered granites (Zhang et al., 2017).

### 6.4. Carbon and oxygen isotopic data for calcite

$\delta^{13}C_{V\text{-}PDB}$ and $\delta^{18}O_{V\text{-}PDB}$ values for calcite from syn-ore stage II veins range from −10.3‰ to −4.3‰ and −22.4‰ to −16.8‰, respectively. The $\delta^{18}O$ and $\delta^{13}C$ values for water and $CO_2$, respectively, in equilibrium with calcite were calculated using the fractionation equations of O'Neil et al. (1969) at a formation temperature of 170 °C (Zhang, 2008). The $\delta^{18}O_{W\text{-}PDB}$ and $\delta^{13}C_{CO2\text{-}PDB}$ values vary from −2.97‰ to +2.83‰ and −11.2‰ to −5.2‰, respectively (Table 4).

The average $\delta^{18}O_{W\text{-}PDB}$ composition of syn-ore fluid in equilibrium with carbonate is 0.5‰, which is within the range of syn-ore fluid in equilibrium with quartz (−1.85‰–5.35‰). The average $\delta^{13}C_{CO2\text{-}PDB}$ of syn-ore fluid in equilibrium with carbonate is −8.6‰. Zhang (2008) interpreted these values to reflect a mantle origin for the ore-forming fluid, which experienced $CO_2$ degassing during U mineralization. The $\delta^{18}O$ values of syn-ore fluid in equilibrium with carbonate are generally negative and correlated with $\delta^{13}C$ values of $CO_2$ in the syn-ore fluid (Fig. 6), apart from sample 1–25 from Zhang (2008). The $\delta^{13}C$ values of syn-ore $CO_2$ are generally close to those of the atmosphere and river, lake, and ocean waters, which means that identification of the $CO_2$ source based only on C isotopic ratios is difficult (Hoefs, 1997).

### 6.5. Sulfur isotopic data for syn-ore pyrite

The $\delta^{34}S_{CDT}$ values of syn-ore stage I and II pyrites range from −3.2‰ to −16.7‰ and −8.1‰ to −17.1‰, respectively. These two stages have a similar wide range of $\delta^{34}S$ values, with three peaks at −17.0‰ to −16.0‰, −11.0‰ to −10.0‰, and −4.0‰ to −3.0‰ (Table 5).

In general, the $\delta^{34}S$ values of the syn-ore pyrites are similar to those for volcanic gas (−20‰–0‰; Zheng and Chen, 2000), which obviously

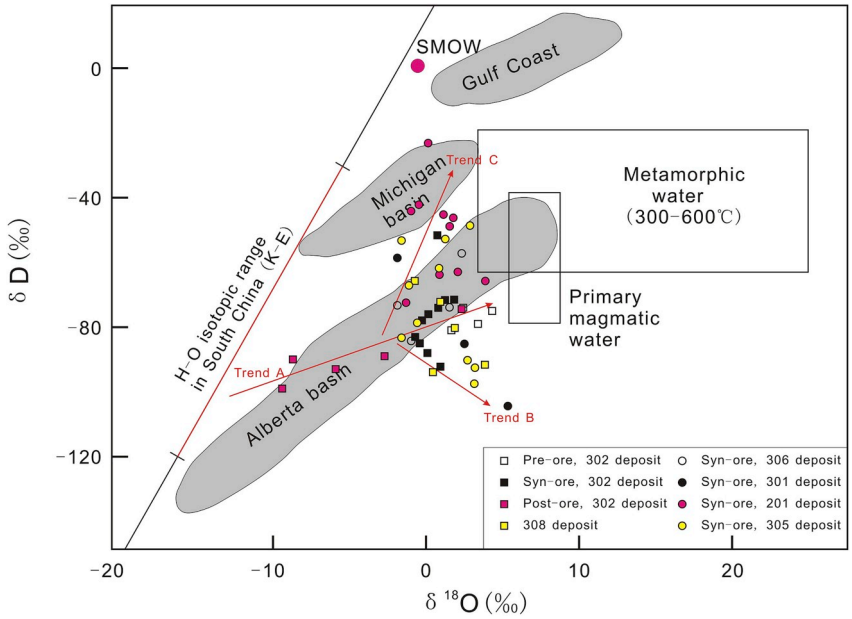


**Fig. 4.** Oxygen-hydrogen isotopic plots of water in equilibrium with quartz, South Zhuguang uranium ore field (Hoefs, 1997; the H-O isotopic range in South China (K–E) is modified from Zhang et al., 1995; the H-O isotopic range of the three basins are modified from Robb, 2005). Data are from Table 1S.

**Table 3**
Oxygen isotope ratios for altered and unaltered granites of South Zhuguang uranium ore field.

| Deposit | Sample No. | Petrology | Distance to orebody | $\delta^{18}O_{V\text{-}SMOW}$(‰) | Reference |
|---|---|---|---|---|---|
| 302 | P22-1 | Altered granite | 0 m | 4.8 | This paper |
| 302 | P22-2 | Altered granite | 1 m | 6.7 | |
| 302 | P22-3 | Altered granite | 2 m | 6.2 | |
| 302 | P22-4 | Altered granite | 10 m | 7.7 | |
| 302 | P22-5 | Altered granite | 15 m | 7.9 | |
| 302 | P22-6 | Altered granite | 20 m | 8.0 | |
| 302 | P22-7 | Altered granite | 30 m | 8.7 | |
| 302 | P22-9 | Unaltered | ~100 m | 13.4 | |
| 306 | 392–3 | Altered granite | 0 m | 3.8 | |
| 306 | 392–4 | Altered granite | 0.5 m | 5.8 | |
| 306 | 392–6 | Altered granite | 3 m | 8.3 | |
| 306 | 392–7 | Altered granite | 5 m | 8.4 | |
| 306 | 392–8 | Altered granite | 10 m | 9.6 | |
| 306 | 392–10 | Altered granite | 20 m | 9.4 | |
| 306 | 392–15 | Altered granite | 30 m | 10.8 | |
| 306 | 392–70 | Altered granite | 50 m | 11.0 | |
| 306 | 392–73 | Unaltered | ~100 m | 12.9 | |
| 301 | ZK01 | Altered granite | 0 m | 4.7 | |
| 301 | ZK02 | Altered granite | 0.5 m | 6.0 | |
| 301 | ZK03 | Altered granite | 1.0 m | 6.8 | |
| 301 | ZK04 | Altered granite | 2.0 m | 7.7 | |
| 301 | ZK05 | Altered granite | 5.0 m | 8.7 | |
| 301 | ZK06 | Altered granite | 10 m | 9.3 | |
| 301 | ZK07 | Altered granite | 15 m | 9.2 | |
| 301 | ZK08 | Altered granite | 20 m | 9.6 | |
| 301 | ZK09 | Altered granite | 30 m | 9.8 | |
| 301 | ZK10 | Altered granite | 50 m | 11.2 | |
| 301 | ZK11 | Unaltered | ~100 m | 11.8 | |
| 201 | L2-54 | Altered granite | 0 m | 3.2 | Li et al. (1995) |
| 201 | L2-101 | Altered granite | 0 m | 4.2 | |
| 201 | L2-53 | Altered granite | 0.5 m | 3.9 | |
| 201 | L2-55 | Altered granite | 1 m | 4.7 | |
| 201 | L2-103 | Altered granite | 1.5 m | 4.3 | |
| 201 | L2-105 | Altered granite | 6.9 m | 4.7 | |
| 201 | L2-61 | Altered granite | 20 m | 6.3 | |
| 201 | L2-108 | Altered granite | 70 m | 6.9 | |
| 201 | L2-111 | Altered granite | 100 m | 8.1 | |
| 201 | L2-202 | Unaltered | 200 m | 11.4 | |

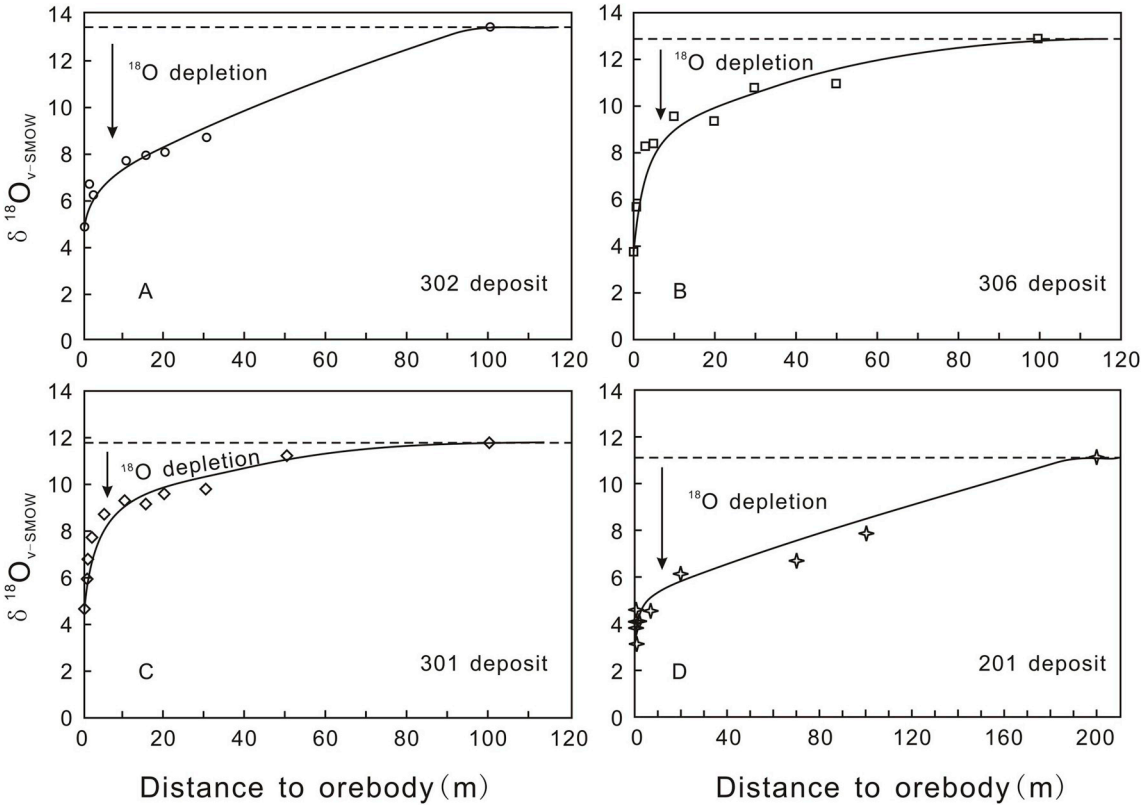


**Fig. 5.** Plots of oxygen isotopic composition of altered granites vs the distance to ore-bearing faults, South Zhuguang uranium ore field. Data are from Table 3.

**Table 4**
The Oxygen and carbon isotopes of syn-ore stage II calcite, 302 deposit, South Zhuguang uranium ore field.

| Sample No. | $\delta^{18}O_{V\text{-}PDB}$(‰) | $\delta^{13}C_{V\text{-}PDB}$(‰) | $\delta^{18}O_{W\text{-}SMOW}$(‰) | $\delta^{13}C_{CO2\text{-}PDB}$(‰) | Temp. (°C) | Reference |
|---|---|---|---|---|---|---|
| 10029–1 | −18.2 | −9.9 | 1.33 | −10.8 | 170 | This paper |
| 04C-2 | −18.0 | −9.9 | 1.63 | −10.8 | 170 | |
| 10029–14 | −19.3 | −7.6 | 0.23 | −8.5 | 170 | |
| 04C-1 | −22.0 | −4.3 | −2.57 | −5.2 | 170 | |
| ZK11-2-2 | −17.9 | −8.2 | 1.63 | −9.1 | 170 | |
| ZK4-4-2 | −16.8 | −10.3 | 2.83 | −11.2 | 170 | |
| 2–14 | −20.09 | −6.9 | −0.57 | −7.8 | 170 | Zhang et al. (2008) |
| 2–15 | −22.41 | −4.3 | −2.97 | −5.2 | 170 | |
| 2–21 | −22.32 | −4.3 | −2.87 | −5.2 | 170 | |
| 3–15 | −22.03 | −4.6 | −2.57 | −5.5 | 170 | |
| 3-26′ | −21.15 | −4.4 | −1.67 | −5.3 | 170 | |
| 1–25 | −17.08 | −4.9 | 2.53 | −5.8 | 170 | |
| 1–21 | −22.32 | −4.4 | −2.87 | −5.3 | 170 | |
| 1–29 | −17.66 | −7.6 | 1.93 | −8.5 | 170 | |
| 3–18 | −18.24 | −7.2 | 1.33 | −8.1 | 170 | |
| 3–33 | −19.79 | −6.7 | −0.27 | −7.6 | 170 | |
| 3–13 | −18.15 | −8.8 | 1.43 | −9.7 | 170 | |
| 3–27 | −19.02 | −9.0 | 0.53 | −9.9 | 170 | |
| 3–26 | −18.15 | −9.2 | 1.43 | −10.1 | 170 | |
| 2–71 | −17.95 | −9.3 | 1.63 | −10.2 | 170 | |
| 2–65 | −18.05 | −8.7 | 1.53 | −9.6 | 170 | |
| 2–18 | −17.18 | −9.4 | 2.43 | −10.3 | 170 | |
| 1–43 | −17.47 | −9.3 | 2.13 | −10.2 | 170 | |
| 1–37 | −17.56 | −9.3 | 2.03 | −10.2 | 170 | |
| 1–38 | −17.56 | −9.8 | 2.03 | −10.7 | 170 | |
| 1–47 | −17.66 | −9.7 | 1.93 | −10.6 | 170 | |

$1000\ln\alpha_{calcite\text{-}H2O} = 2.78 \times 10^6 T^{-2} - 3.39$ (0–500 °C) (O´;Neil et al., 1969).

is not a plausible S source, given there was no magmatism in the South Zhuguang area during U mineralization (Zhang et al., 2018a). The identification of the S source is difficult using only S isotopic data.

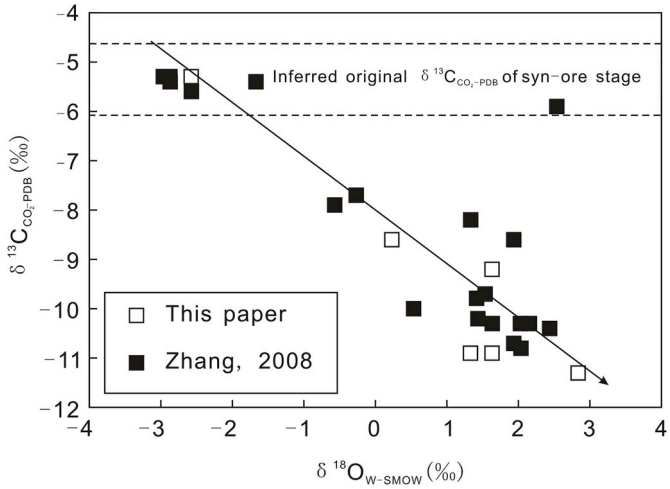


**Fig. 6.** The $\delta^{18}O_{W\text{-}SMOW}$ values of water against to $\delta^{13}C_{CO2\text{-}PDB}$ values, both of which are in equilibrium with carbonate, respectively, South Zhuguang uranium ore field. Data are from Table 4.

Our data indicate that in the ore-forming fluid, S existed mainly as $SO_4^{2-}$ and not $S^{2-}$ or $HS^-$. The $SO_4^{2-}$ was reduced to $S^{2-}$ and then formed pyrite ($FeS_2$). This inference is supported by laser Raman analyses of fluid inclusions, which identified $SO_2$ but almost no $H_2S$ (Zhang, 2008; Zhang et al., 2017). $\delta^{34}S_{CDT}$ values for pyrite are < 0‰ and span a wide range (Fig. 7), which suggest that isotopic equilibrium between $SO_4^{2-}$ in the hydrothermal fluid and pyrite was not attained or that there was considerable fractionation of S isotopes between fluid $SO_4^{2-}$ and pyrite (Ohmoto and Rye, 1979; Ohmoto and Goldhaber, 1997).

Inferring the S isotopic composition of a hydrothermal fluid from $\delta^{34}S_{CDT}$ values of hydrothermal sulfides requires a number of factors to

**Table 5**
The Sulfur isotopes of South Zhuguang uranium ore field.

| Sample No. | Deposit | Mineral | Description | $\delta^{34}S_{V\text{-}CDT}$(‰) | Reference |
|---|---|---|---|---|---|
| 10002–3 | 306 | Pyrite | Syn-ore stage I | −9.6 | This paper |
| 10002–4 | 306 | Pyrite | Syn-ore stage II | −14.0 | |
| 15002–3 | 306 | Pyrite | Syn-ore stage II | −10.6 | |
| 15002–2 | 306 | Pyrite | Syn-ore stage II | −8.3 | |
| GZN201-1 | 302 | Pyrite | Syn-ore stage I | −3.2 | |
| ZK4-2-8 | 302 | Pyrite | Syn-ore stage I | −3.5 | |
| 199–1 | 302 | Pyrite | Syn-ore stage I | −16.7 | |
| 201–11 | 302 | Pyrite | Syn-ore stage I | −9.7 | |
| ZK11-2-2 | 302 | Pyrite | Syn-ore stage I | −10.7 | |
| GZN201-03 | 302 | Pyrite | Syn-ore stage II | −9.1 | |
| GZN201-05 | 302 | Pyrite | Syn-ore stage II | −17.1 | |
| 198–1 | 302 | Pyrite | Syn-ore stage II | −16.5 | |
| ZN43-2 | 302 | Pyrite | Syn-ore stage II | −16.3 | |
| ZN47-1 | 302 | Pyrite | Syn-ore stage II | −8.2 | |
| ZN47-2 | 302 | Pyrite | Syn-ore stage II | −8.1 | |
| ZN47-4 | 302 | Pyrite | Syn-ore stage II | −10.1 | |
| ZN47-5 | 302 | Pyrite | Syn-ore stage II | −9.9 | |
| 3–31 | 302 | Pyrite | Syn-ore | −10.1 | Zhang (2008) |
| 3–72 | 302 | Pyrite | Syn-ore | −11.9 | |
| 3–78 | 302 | Pyrite | Syn-ore | −14.4 | |
| 3–79 | 302 | Pyrite | Syn-ore | −13.2 | |
| 3–34 | 302 | Pyrite | Syn-ore | −15.5 | |
| 3–43 | 302 | Pyrite | Syn-ore | −15.3 | |
| DZ-S204 | 302 | Pyrite | Syn-ore | −10.2 | Huang (1996) |
| DZ-S205 | 302 | Pyrite | Syn-ore | −10.2 | |
| DZ-S207 | 302 | Pyrite | Syn-ore | −8.9 | |
| DZ-S221 | 302 | Pyrite | Syn-ore | −9.8 | |
| DZ-S220 | 302 | Pyrite | Syn-ore | −8.0 | |
| DZ-S113 | 302 | Pyrite | Syn-ore | −7.8 | |
| DZ-S209 | 302 | Pyrite | Syn-ore | −9.5 | |
| No.1 | 302 | Pyrite | Syn-ore | −7.0 | Hu (1984) |
| No.2 | 302 | Pyrite | Syn-ore | −4.6 | |
| L2-303 | 201 | Pyrite | Syn-ore | −8.9 | Li et al. (1995) |
| L2-304 | 201 | Pyrite | Syn-ore | −7.3 | |
| L2-244 | 201 | Pyrite | Syn-ore | −10.2 | |
| L2-250 | 201 | Pyrite | Syn-ore | −11.3 | |
| L2-267 | 201 | Pyrite | Syn-ore | −12.3 | |
| L2-302 | 201 | Pyrite | Syn-ore | −10.1 | |
| L2-280 | 201 | Pyrite | Syn-ore | −14.5 | |

be considered, including: (1) the temperature of deposition; (2) the chemical composition of the dissolved element species, as well as the pH and $fO_2$, at the time of mineralization; and (3) the relative amount of the mineral deposited from the fluid (Zheng and Hoefs, 1993; Zheng and Chen, 2000). Previous microthermometric studies have determined that sulfides were generally deposited at 200–300 °C from the ore-forming fluid (Zhang, 2008; Zhang et al., 2017), which means the $\delta^{34}S_{CDT}$ values of pyrite might generally represent the $\delta^{34}S_{CDT}$ values of $H_2S$ in the ore-forming fluid (Ohmoto and Goldhaber, 1997), but not the isotopic composition of $SO_4^{2-}$. In the ore-forming fluid, $SO_4^{2-}$ was the dominant S species, and it experienced pH and $fO_2$ variations (Zhang, 2008; Zhang et al., 2017), which transformed the $SO_4^{2-}$ into $H_2S$. The reasons for the pH and $fO_2$ variations are considered in Section 7.2. During U mineralization, the ore-forming fluid was subjected to an increase in pH and decrease in $fO_2$ (Zhang et al., 2017). Hoefs (1997) showed that an increase in pH leads directly to an increase in the $\delta^{34}S_{CDT}$ values of precipitated sulfides, and a decrease in $fO_2$ has a much stronger effect on the $\delta^{34}S_{CDT}$ values than a pH change, because of the large S isotopic fractionation between sulfate and sulfide. When high $fO_2$ values allow the proportion of sulfate species to become significant, mineral $\delta^{34}S_{CDT}$ values can be very different from the $\delta^{34}S_{CDT}$ values of the fluid, and small changes in pH or $fO_2$ may result in large changes in the S isotopic composition of sulfide or sulfate (Ohmoto and Rye, 1979; Ohmoto and Goldhaber, 1997). In addition, when sulfide minerals precipitate from fluids, S isotopic fractionation occurs between dissolved S species and sulfide minerals. The removal of sulfide from fluids in a closed system can cause a measureable isotopic fractionation in the $H_2S$ remaining in the fluids. In summary, the three aforementioned factors are responsible for the $\delta^{34}S_{CDT}$ variations of sulfides from the South Zhuguang U field (Drummond and Ohmoto, 1985; McKibben and Eldridge, 1990).

### 6.6. Strontium isotopic data

The $^{87}Sr/^{86}Sr$ values of ore-hosting granites, and syn-ore stage I and post-ore fluorites are 0.780939–0.954319, 0.719250–0.721327, and 0.716299–0.714598, respectively, with $^{87}Rb/^{86}Sr$ values of 17.6–109.0, 0.0387–0.0524, and 0.0120–0.0446, respectively. The $^{87}Sr/^{86}Sr$ values of pitchblende are 0.719771–0.723121, but only one $^{87}Rb/^{86}Sr$ analysis (0.6551) was provided by Zhang (2008) (Table 6).

The initial $^{87}Sr/^{86}Sr$ ratios (calculated at 54 Ma) of syn- and post-ore fluorites vary widely from 0.719250 to 0.721327 and 0.714598 to 0.716299, respectively. Plots of initial $^{87}Sr/^{86}Sr$ values against 1/Sr suggest mixing between syn- and post-ore fluorites (Fig. 8; trend C in Fig. 9; Faure, 1986), even though the analyzed fluorites were hand-picked. This mixing trend may reflect the overprinting of post-ore fluids on syn-ore fluorite, although this is not evident from microscopic observations. The initial $^{87}Sr/^{86}Sr$ ratios of syn- and post-ore fluorites are generally ~0.7215 and ~0.7145, respectively. $^{87}Sr/^{86}Sr$ ratios of pitchblende have a wider range than these initial $^{87}Sr/^{86}Sr$ ratios (~0.7211–0.7217; Fig. 9), which likely results from the high Rb contents of the pitchblende (trend A in Fig. 9) and overprinting by post-ore fluids (trend B in Fig. 9). In addition, sample 2-70-1 (Zhang, 2008) has a higher initial $^{87}Sr/^{86}Sr$ than the syn-ore fluorites, which probably reflects the incorporation of granite fragments during pitchblende deposition. The initial $^{87}Sr/^{86}Sr$ ratios of the ore-hosting granites are much higher than those of the syn-ore fluorites (Fig. 8), which rules out the possibility that the ore-forming fluids were sourced directly from the granites.

## 7. Discussion

### 7.1. Uranyl complexes in the ore-forming fluid

The identification of $O_2$ in fluid inclusions by laser Raman analyses indicates that the ore-forming fluid had a high oxygen fugacity (Zhang et al., 2017). At temperatures of > 200 °C, theoretical calculations indicate that in relatively oxidizing brines, $U^{6+}$ exists mainly as carbonate complexes at high pH, phosphate complexes at neutral pH, fluoride and chloride complexes at low pH, and sulfate complexes at very low pH (Cuney and Kyser, 2008). As the temperature increases, hydroxyl complexes become dominant, particularly at high pH, but phosphate complexes remain dominant at neutral pH despite the emergence of important hydroxyl complexes (Romberger, 1984; Cuney and Kyser, 2008). In the South Zhuguang U ore field, bulk volatile and ionic compositions, and microthermometric and laser Raman analyses of fluid inclusions suggest that the uranyl complexes in the ore-forming fluid were somewhat different to those documented in previous studies.

During syn-ore stage I, the ore-forming fluid was acidic, which rules out the presence of carbonate or hydroxide complexes. The dominant anionic species were $SO_4^{2-}$ and $F^-$, and the content of $Cl^-$ was much smaller than that of $F^-$ (Table 1), which suggests that $UO_2F_3^-$, $UO_2F_4^{2-}$, $UO_2F_2$, and $UO_2SO_4$ were the main uranyl complex species. In syn-ore stage II, the ore-forming fluid was alkaline, which means that carbonate and hydroxide complexes ($UO_2(OH)_3^-$ and $UO_2(OH)_2$) were probably the dominant uranyl species at temperatures of 200–250 °C (Romberger, 1984; Kojima et al., 1994; Bernhard et al., 2001).

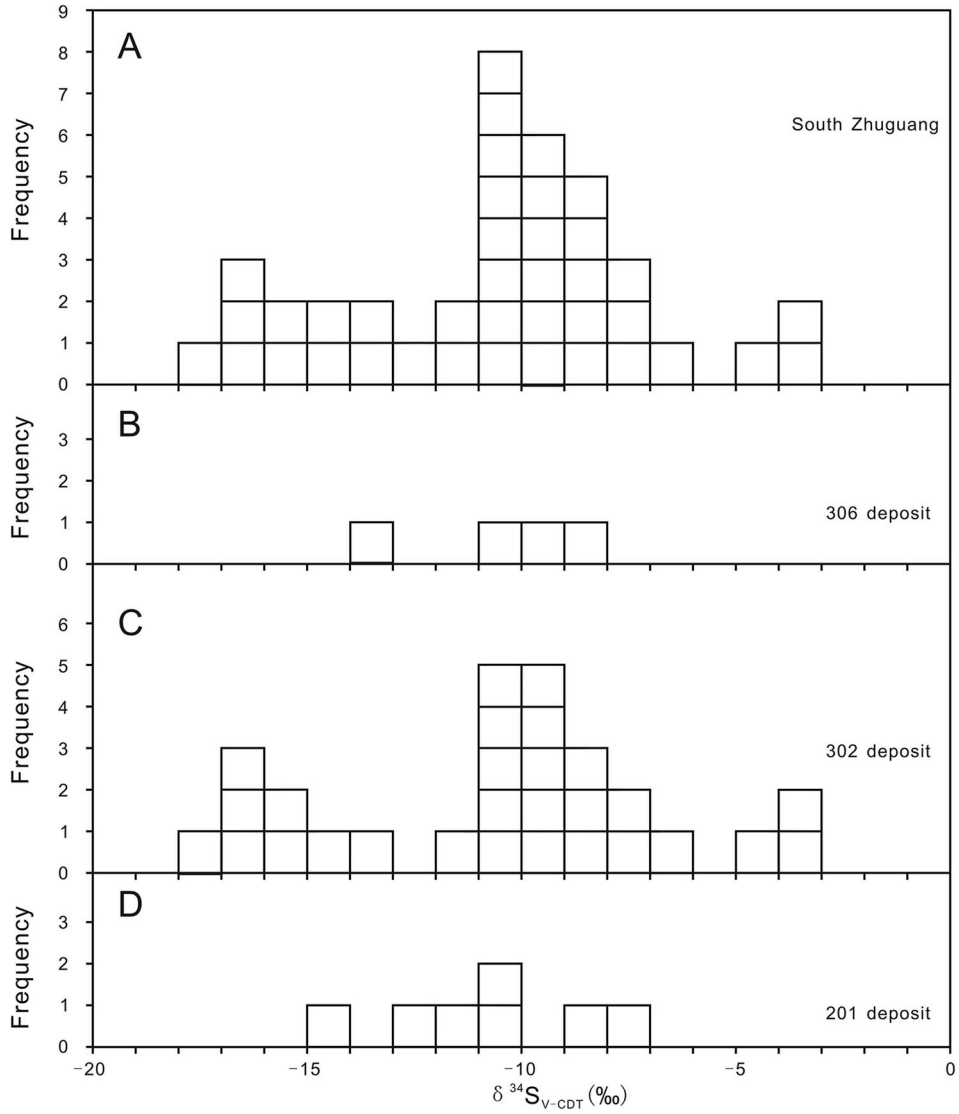


**Fig. 7.** Sulfur isotope histogram for the syn-ore pyrites in South Zhuguang uranium ore field (A), 306 deposit (B), 302 deposit (C), 201 deposit (D). Data are from Table 5.

### 7.2. Water–rock interactions between fluid and ore-hosting granites

Before considering the source of the ore-forming fluids, water–rock interactions between the fluids and ore-hosting granites need to be considered. For example, the progressive $^{18}O$ depletion of altered granites (Fig. 5) indicates that a large amount of $^{18}O$ was transported into the ore-forming fluid during mineralization, which would have increased the $\delta^{18}O$ values of the ore-forming fluid.

In the South Zhuguang U ore field, the alteration adjacent to the ore-bearing faults resulted in plagioclase and K-feldspar being altered into fine-grained sericite (hydromica) and quartz, and biotite being altered into chlorite and hematite, according to the following chemical reactions (Robb, 2005):

**plagioclase + $K^+$ + $H^+$ → sericite + quartz + $Na^+$ + $Ca^{2+}$**

*(pH increase and $Ca^{2+}$ release into the ore-forming fluid)*

$3NaAlSi_3O_8 + K^+ + 2H^+ \rightarrow KAl_3Si_3O_{10}(OH)_2 + 6SiO_2 + 3Na^+$

$3CaAl_2Si_2O_8 + 2K^+ + 4H^+ \rightarrow 2KAl_3Si_3O_{10}(OH)_2 + 3Ca^{2+}$

**plagioclase + $H_2O$ + $K^+$ + $H^+$ → illite + quartz + $Na^+$ + $Ca^{2+}$**

*(pH increase and $Ca^{2+}$ release into the ore-forming fluid)*

$3NaAlSi_3O_8 + xH_2O + (1 - x)K^+ + (2 + x)H^+ \rightarrow K_{1-x}(H_2O)_x\{Al_2[AlSi_3O_{10}](OH)_{2-x}(H_2O)_x\} + 6SiO_2 + 3Na^+$

$3CaAl_2Si_2O_8 + 2xH_2O + (2–2x)K^+ + (4 + 2x)H^+ \rightarrow 2K_{1-x}(H_2O)_x\{Al_2[AlSi_3O_{10}](OH)_{2-x}(H_2O)_x\} + 3Ca^{2+}$

**K-feldspar + $H^+$ → sericite + quartz + $K^+$**

*(pH increase)*

$3KAlSi_3O_8 + 2H^+ \rightarrow KAl_3Si_3O_{10}(OH)_2 + 6SiO_2 + 2K^+$

**K-feldspar + $H_2O$ + $H^+$ → illite + quartz + $K^+$**

*(pH increase)*

$3KAlSi_3O_8 + xH_2O + (2 + x)H^+ \rightarrow K_{1-x}(H_2O)_x\{Al_2[AlSi_3O_{10}](OH)_{2-x}(H_2O)_x\} + 6SiO_2 + (2 + x)K^+$

**biotite + $O_2$ (details in fluid inclusions) → chlorite + hematite**

*(oxygen fugacity decrease that resulted in reduction of $U^{6+}$ to $U^{4+}$)*

$K\{(Mg_{<0.67},Fe_{>0.33})_3[AlSi_3O_{10}](OH)_2\} + O_2 \rightarrow (Mg,Fe)_{5–6}$

**Table 6**
Rb-Sr isotopes for South Zhuguang uranium ore field.

| Mineral | Deposit | Sample No. | Rb(ppm) | Sr(ppm) | $^{87}Rb/^{86}Sr$ | $^{87}Sr/^{86}Sr(2\sigma)$ | $(^{87}Sr/^{86}Sr)_i$ | $Rb(ppm)_i$ | $Sr(ppm)_i$ | $(^{87}Rb/^{86}Sr)_i$ | Reference |
|---|---|---|---|---|---|---|---|---|---|---|---|
| Syn-ore | 301 | 025–0 | 0.422 | 47.1 | 0.0401 | 0.720558(11) | 0.720527 | 0.422 | 47.1001 | 0.0401 | This paper |
| Stage I | | 025–1 | 0.517 | 43.6 | 0.0387 | 0.720901(12) | 0.720871 | 0.517 | 43.6001 | 0.0387 | |
| Fluorite | | GZN202-2 | 0.527 | 43.7 | 0.0419 | 0.721359(12) | 0.721327 | 0.527 | 43.7001 | 0.0419 | |
| | | −15005 | 0.625 | 52.8 | 0.0524 | 0.71929(10) | 0.71925 | 0.625 | 52.8001 | 0.0524 | |
| | | 203–3 | 0.754 | 42.3 | 0.0453 | 0.721038(12) | 0.721003 | 0.754 | 42.3002 | 0.0453 | |
| Post-ore | | ,9C04 | 0.906 | 90.2 | 0.0446 | 0.715045(14) | 0.715011 | 0.906 | 90.2002 | 0.0446 | |
| Fluorite | | 9C12 | 0.834 | 92.4 | 0.0184 | 0.715036(11) | 0.715022 | 0.834 | 92.4002 | 0.0184 | |
| | | ZK4-3-17 | 0.526 | 87.8 | 0.0296 | 0.715986(12) | 0.715963 | 0.526 | 87.8001 | 0.0296 | |
| | | ZK4-3-8 | 0.553 | 74.5 | 0.0317 | 0.716323(14) | 0.716299 | 0.553 | 74.5001 | 0.0317 | |
| Syn-ore | 302 | 3–02 | 1.27 | 89.7 | 0.0409 | 0.715364(11) | 0.715333 | 1.270 | 89.7003 | 0.0409 | Zhang (2008) |
| Stage I | | 3–28 | 0.749 | 47.3 | 0.0459 | 0.720285(15) | 0.72025 | 0.749 | 47.3002 | 0.0459 | |
| Fluorite | | 3–21 | 0.863 | 59.5 | 0.0420 | 0.714630(15) | 0.714598 | 0.863 | 59.5002 | 0.0420 | |
| | | 3–48 | 0.346 | 83.8 | 0.0120 | 0.715905(13) | 0.715896 | 0.346 | 83.8001 | 0.0120 | |
| | | 3–49 | 0.526 | 93.7 | 0.0162 | 0.715391(13) | 0.715379 | 0.526 | 93.7001 | 0.0162 | |
| | | 3–50 | 0.769 | 94.5 | 0.0235 | 0.715403(14) | 0.715385 | 0.769 | 94.5002 | 0.0235 | |
| Pitchblende | 302 | 2-70-1 | 16.1 | 71.0 | 0.6551 | 0.723056(12) | 0.722554 | 16.097 | 71.0035 | 0.6556 | |
| | | 2-70-2 | – | – | – | 0.723121(13) | | | | | |
| | | 3–31 | – | – | – | 0.719771(12) | | | | | |
| | | 3–34 | – | – | – | 0.722754(12) | | | | | |
| | | 3–78 | – | – | – | 0.721754(12) | | | | | |
| Ore-hosting granite | 302 | 3–57 | 379 | 63.0 | 17.6 | 0.780939(14) | 0.767443 | 378.918 | 63.0822 | 17.6135 | |
| | | 3–56 | 391 | 59.6 | 19.1 | 0.791201(14) | 0.776555 | 390.915 | 59.6848 | 19.1146 | |
| | | 2–24 | 464 | 12.7 | 109 | 0.954319(15) | 0.870738 | 463.899 | 12.8007 | 109.0836 | |
| | | 3–37 | 481 | 45.7 | 30.8 | 0.818082(13) | 0.794465 | 480.896 | 45.8044 | 30.8236 | |
| | | 2–38 | 422 | 39.7 | 31.0 | 0.790208(13) | 0.766437 | 421.908 | 39.7916 | 31.0238 | |

$(^{87}Sr/^{86}Sr)_i$: the $^{87}Sr/^{86}Sr$ ratios at 54 Ma; $Rb(ppm)_i$: the Rb contents at 54 Ma; $Sr(ppm)_i$: the Sr contents at 54 Ma; $(^{87}Rb/^{86}Sr)_i$: the $^{87}Sr/^{86}Sr$ ratios at 54 Ma.

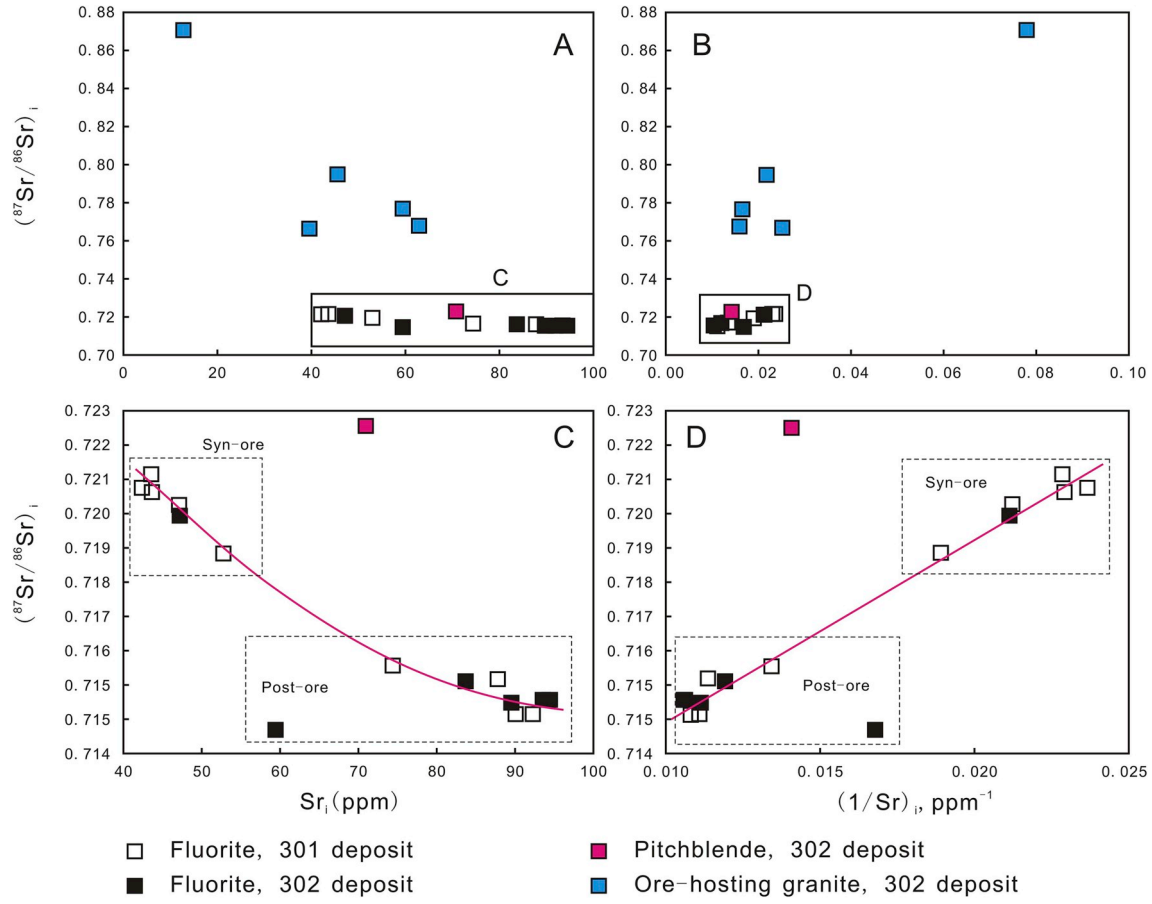


**Fig. 8.** Plots of initial $(^{87}Sr/^{86}Sr)$ ratios vs the Sr contents and 1/(Sr contents) showing the mixing of syn-ore and post-ore fluorites (part data sourced from Zhang, 2008). Data are from Table 6.

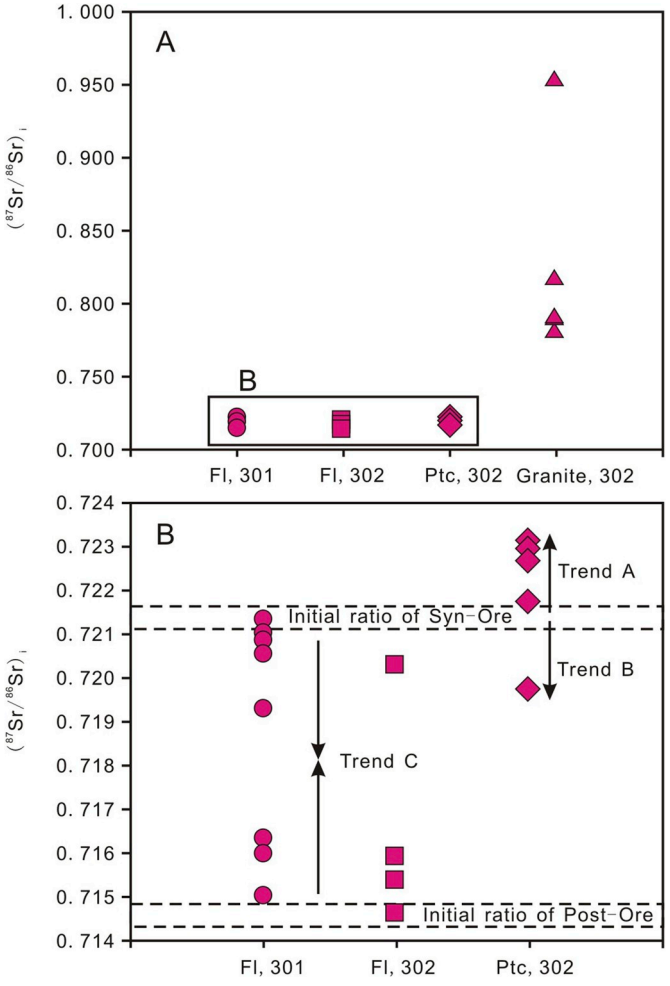


**Fig. 9.** Plots of $(^{87}Sr/^{86}Sr)_i$ for syn-ore and post ore fluorite, and pitchblende, South Zhuguang uranium ore field (part data sourced from Zhang, 2008) that showing the interfusion of granite fragments during deposition of pitchblende (Trend A), the superimposition of post-ore fluid on pitchblende (Trend B), and the mix of syn-ore and post-ore fluorites (Trend C). Data are from Table 6.

$$[(Al,Si)_4O_{10}](OH)_8 + Fe_2O_3 + K^+$$

The above chemical reactions suggest the ore-forming fluid was oxidizing and acidic (at least for syn-ore stage I), and its pH and chemistry would have changed significantly during hydrothermal alteration, with the exception of its O–H–Sr isotopic compositions. Illitization, chloritization, and hematization would have increased the pH and decreased the oxygen fugacity of the ore-forming fluid, and released large amounts of $Ca^{2+}$ and probably $F^-$ from the ore-hosting granites (Robb, 2005; Deng et al., 2013, 2014).

The O and H isotopic compositions of the syn-ore fluids were influenced by alteration (Fig. 4). Fractionation factors between sericite, illite, chlorite, and water are all < 1 (Sheppard, 1986; Hoefs, 1997; Zheng and Chen, 2000) at mineralization temperatures of 200–300 °C (Zhang, 2008; Zhang et al., 2017).

Unlike O–H isotopes, the C and S isotopic compositions of syn-ore calcite and pyrite, respectively, are only influenced to a small extent by hydrothermal alteration. This means the C–S isotopic data might broadly represent the syn-ore fluids, given the much lower C–S contents of the ore-hosting granites relative to the ore-forming fluid. However, the $^{87}Sr/^{86}Sr$ ratios of the syn- and post-ore fluids were probably significantly affected by hydrothermal alteration, due to the wide range of initial $^{87}Sr/^{86}Sr$ ratios and high Sr contents of the ore-hosting granites. Although accurate $^{87}Sr/^{86}Sr$ ratios for the syn- and post-ore fluids cannot be obtained, these were likely lower than the measured fluorite values.

### 7.3. Mineralization processes

The ore-forming fluids in the South Zhuguang U ore field can be divided into two stages: (1) stage 1 fluids that were acidic and oxidizing, containing fluoride and sulfate complexes of $UO_2^{2+}$ as the dominant species; and (2) stage 2 fluids that were alkaline and oxidizing, containing carbonate and hydroxide complexes of $UO_2^{2+}$ as the dominant transport species. The mineralization mechanisms varied in each stage, due to the different types of ore-forming fluid.

During stage I, hydrothermal alteration (illitization, hematization, chloritization, and silicification) played a key role in controlling U mineralization and was probably associated with the reduction of $SO_4^{2-}$ in the ore-forming fluid by $Fe^{2+}$ and $CO_2$ degassing, as follows:

$$8H_2O + SO_4^{2-} + 8Fe^{2+} = 4Fe_2O_3(\downarrow) + H_2S(\uparrow \text{ with } CO_2 \text{ vapor}) + 14H^+ \text{ (neutralized by illitization)}.$$

Hydrothermal alteration would have released large amounts of $Ca^{2+}$ and $F^-$ into the ore-forming fluid (Li and Jiang, 1992; Robb, 2005; Deng et al., 2013, 2014) and increased the pH of the hydrothermal fluid. The increase in the pH and $Ca^{2+}$ contents of the ore-forming fluid would probably have resulted in the formation of fluorite veins, due to which the uranyl complex species of $UO_2F_3^-$, $UO_2F_4^{2-}$, and $UO_2F_2$ would have decomposed and lowered the saturation solubility of uranyl. The reduction of the ore-forming fluid was also responsible for the conversion of $U^{6+}$ to $U^{4+}$, both of which led to a drastic decrease in U solubility and the formation of pitchblende–fluorite–quartz veins of syn-ore stage I, as follows:

$$H^+ + UO_2(SO_4) + Fe^{2+} \text{ (biotite)} + Ca^{2+} + UO_2(F^-)_n^{(n-2)-} \rightarrow UO_2(\downarrow) + Fe_2O_3(\downarrow) + CaF_2(\downarrow) + FeS_2(\downarrow) + H_2S(\uparrow \text{ with } CO_2 \text{ vapor}) + H_2O.$$

However, the pitchblende–quartz–calcite veins of syn-ore stage II imply another U mineralization process. Uranyl carbonate $(UO_2(CO_3)^{2-})$ and hydroxide complexes $(UO_2(OH)_3^-$ and $UO_2(OH)_2)$ were dominant in hydrothermal fluids of syn-ore stage II (Romberger, 1984; Kojima et al., 1994), which experienced relatively oxidizing and high pH conditions at temperatures of ~200 °C. Zhang (2008) and Zhang et al. (2017) suggested $CO_2$ degassing during hydrothermal alteration. Carbon dioxide (and $H_2S$) loss leads to a pH increase in the residual fluids, which causes calcite precipitation (Franco, 2009). In addition, during syn-ore stage II there was also reduction of the ore-forming fluid, as indicated by the occurrence of pyrite, which resulted from the reduction of $SO_4^{2-}$ in the ore-forming fluid. The $CO_2$ degassing would have decomposed the carbonate complexes $(UO_2(CO_3)^{2-})$ and led to the deposition of pitchblende–calcite–quartz veins (Langmuir, 1978; Tripathi, 1979; Romberger, 1984; Kojima et al., 1994), as follows:

$$Ca^{2+} + UO_2(CO_3) + SO_4^{2-} + UO_2(OH)_3^- + Fe^{2+} + HCO_3^- \rightarrow UO_2(\downarrow) + Fe_2O_3(\downarrow) + FeS_2(\downarrow) + CaCO_3(\downarrow) + OH^- + CO_2(\uparrow).$$

### 7.4. Source of the ore-forming fluid

The O–H–C–S isotopic data for the South Zhuguang U ore field can be interpreted in a number of ways, particularly if the geological background and mineralization processes are not considered. The mineralization ages of 52–57 Ma (Zhang, 2008; Zhang et al., 2018a) obtained from U–Pb isochron dating of pitchblende rule out the possibilities that the fluid was sourced from the ore-hosting granites or weakly metamorphosed country rocks, given the U mineralization is tens or hundreds of millions of years younger than granite emplacement and regional metamorphism.

The measured $\delta^{18}O_{W\text{-}SMOW}$ and $\delta D_{W\text{-}SMOW}$ values of the ore-forming fluid are the result of modification of the original U-bearing fluid by fluid–rock interactions with the ore-hosting granites and $CO_2$ degassing during U mineralization (Zhang, 2008; Zhang et al., 2017). The fluid–rock interactions would have increased the $\delta^{18}O$ and $\delta D$ values of the ore-forming fluid by isotopic exchange with the granites, and given the isotopic fractionation factors (< 1; Zheng and Chen, 2000) between the main igneous–alteration minerals and water at the temperatures of U mineralization (generally 150–350 °C; Zhang, 2008; Zhang et al., 2017). The effects of $CO_2$ degassing on $\delta^{18}O$ and $\delta D$ values of the ore-forming fluid depend on the temperature. During $CO_2$ degassing, there would have been a large amount of $H_2O$ vapor associated with $CO_2$ loss. This process would have increased the $\delta^{18}O$ values of the ore-forming fluid, whereas the effect on $\delta D$ values would have depended on temperature (Horita and Wesolowski, 1994; Hoefs, 1997). If temperatures were < 220 °C, then the fractionation between the vapor and liquid phase of water would have increased the $\delta D$ values of the ore-forming fluid, whereas at 230–350 °C the fluid would have become more depleted in D, and at 220–230 °C there would have been little D/H fractionation. Considering this, the scatter in the O–H isotopic data for the ore-forming fluid can be readily understood. In Fig. 4, trend B represents $CO_2$ degassing at temperatures of < 220 °C, and trend C reflects the combined effects of fluid–rock interactions and $CO_2$ degassing at temperatures of > 230 °C. The ore-forming fluid had a close resemblance to basinal fluids, particularly those formed in extensive evaporitic environments (Fig. 4; Gat, 1984), consistent with a Cretaceous–Paleogene redbed basin source (trend A in Fig. 4), when the effects of later alteration are taken into account.

Without the H–O isotopic evidence from the ore-forming fluids, the linear correlation between $\delta^{13}C_{V\text{-}PDB}$ and $\delta^{18}O_{V\text{-}PDB}$ values of syn-ore calcite could be interpreted in three ways: (1) subequal mixing of two different fluids; (2) a decrease in $\delta^{18}O_{V\text{-}SMOW}$ values associated with a $\delta^{13}C_{V\text{-}PDB}$ increase; or (3) an increase in $\delta^{18}O_{V\text{-}SMOW}$ values associated with a $\delta^{13}C_{V\text{-}PDB}$ decrease, due to some geological process (Zheng and Hoefs, 1993; Hoefs, 1997). Given that the $^{18}O$ content of the ore-forming fluid generally increased during U mineralization, we prefer the explanation outlined in (3). The variations in $\delta^{13}C_{CO2\text{-}PDB}$ were caused mainly by $CO_2$ degassing, which was a common process during formation of the South Zhuguang U ore field (Zhang, 2008; Zhang et al., 2017). The C-bearing components in the ore-forming fluid probably contained $FeCO_3$, $CaMg(CO_3)_2$, $CaCO_3$, and $HCO_3^-$, but given that only the fractionation factor between $HCO_3^-$ and $CO_2$ is smaller than 1 at the mineralization temperature, the C-bearing component must have been predominantly $HCO_3^-$ in addition to $CO_2$ (Zheng and Hoefs, 1993). Accompanied by the release of $Ca^{2+}$ into the ore-forming fluid from the ore-hosting granite during alteration, the $CO_2$ degassing would have led to calcite deposition with pitchblende, as follows:

$$Ca^{2+} + 2HCO_3^- = CaCO_3(\downarrow) + H_2O + CO_2(\uparrow).$$

After accounting for the effects of $CO_2$ degassing, the $\delta^{13}C$ values of syn-ore stage II $CO_2$ are nearly the same as those of a basinal fluid (−5‰; Zheng and Chen, 2000). This is again consistent with a Cretaceous–Paleogene redbed basin source for the ore-forming fluids (Fig. 6).

The S-bearing component in the original ore-forming fluid sourced from the redbed basins is likely to have been predominantly $SO_4^{2-}$, given the high oxygen fugacity inferred from the $O_2$ in the syn-ore fluid inclusions (Zhang et al., 2017). As such, the $\delta^{34}S_{CDT}$ values of the syn-ore pyrites are the result of at least two processes: (1) the transformation of $SO_4^{2-}$ into $S^{2-}$ by a redox process; and (2) equilibrium isotopic fractionation between $S^{2-}$ in the hydrothermal fluid and pyrite at mineralization temperatures of 150–350°. The redox process (1) was associated with chloritization of biotite and $CO_2$ degassing, which means the $S^{2-}$ was probably lost as $H_2S$ along with $CO_2$ vapor, because the pH of the ore-forming fluid was low (syn-ore stage I), as follows:

$$H^+ + SO_4^{2-} + Fe^{2+}\ (\text{biotite}) \rightarrow Fe_2O_3(\downarrow) + H_2S(\uparrow \text{ with } CO_2 \text{ vapor}).$$

The release of $H_2S$ vapor would have prevented isotopic equilibrium in the hydrothermal fluid between $S^{2-}$ and $SO_4^{2-}$, as well as between the $S^{2-}$ in the hydrothermal fluid and pyrite (2). This is consistent with the wide range of $\delta^{34}S_{CDT}$ values of syn-ore pyrites (Fig. 7). Given the increase in pH and decrease in oxygen fugacity of the ore-forming fluid during alteration, the syn-ore pyrites should have $\delta^{34}S_{CDT}$ values 22.8‰ higher than those of $SO_4^{2-}$ in the ore-forming fluid, if isotopic equilibrium was attained at 250 °C (Ohmoto, 1972; Hoefs, 1997). The $\delta^{34}S_{CDT}$ values of the pyrites range from −17.1‰ to −3.2‰, and therefore the $\delta^{34}S_{CDT}$ values of $SO_4^{2-}$ in the original ore-forming fluids were +5.7‰ to +19.6‰, similar to the values in river and ocean waters (Zheng and Chen, 2000). As such, basinal fluids sourced from the Cretaceous–Paleogene redbed basins were also responsible for pyritization in the South Zhuguang U ore field.

The fluorite Sr isotopic data were unaffected by $CO_2$ degassing, but were affected by hydrothermal alteration. The $(^{87}Sr/^{86}Sr)_i$ ratios of syn-ore stage I and post-ore fluorites are generally 0.719250–0.721327 and 0.714598–0.716299, respectively (Figs. 8 and 9), much lower than those of the ore-hosting granites. Clearly, the $(^{87}Sr/^{86}Sr)_i$ ratios of syn-ore stage I and post-ore fluorites are the result of interactions between the ore-forming fluid and ore-hosting granites (Faure, 1986), which suggests the $(^{87}Sr/^{86}Sr)_i$ ratios of the original fluids were even lower than the above values. In the South Zhuguang area, only the Sinian–Carboniferous limestone has lower $(^{87}Sr/^{86}Sr)_i$ ratios (~0.70967) than the fluorites (Wu, 1985; Li, 1992). The $(^{87}Sr/^{86}Sr)_i$ ratios of the nearby granites, sandstones, mudstones, and conglomerates are generally 0.76164–0.870738, much higher than the $(^{87}Sr/^{86}Sr)_i$ ratios of the fluorites. The Cretaceous–Paleogene redbed basins provide a suitable setting for the interaction between basinal fluids and Sinian–Carboniferous limestone, particularly given the soluble nature of the limestone, and this accounts for the low $(^{87}Sr/^{86}Sr)_i$ ratios of the basinal fluids and syn-ore stage I and post-ore fluorites.

Initially, the basinal fluids would have been mainly meteoric water, characterized by high oxygen fugacities (Zhang et al., 2017) that would have enabled the fluids to easily extract U, other ions (e.g., $F^-$, $Cl^-$, $NO_3^-$, $Mg^{2+}$, and $K^+$), and gases (e.g., $CH_4$ and $CO_2$) from terrigenous clasts through water–rock interactions (Maynard, 1991; Kyser et al., 2000; Cuney et al., 2003). These clasts would have originated mainly from the surrounding granites and metamorphic basement, and had a high effective surface area, which was five to seven orders of magnitude greater than that of the granite body. The ore-forming fluids might have migrated through the metamorphic basement rocks (Fig. 10), along regional faults, to sites of mineralization in the sedimentary basins.

Previous studies have proposed that ore-forming fluids in some hydrothermal-type U deposits in South China contained mantle-derived gaseous components, based on He, Ar, and C isotopic analysis (e.g., the Xiangshan U district; Hu et al., 2008, 2009). If the ore-forming fluid of the Xiangshan U district was also sourced from the Gan–Hang redbed basin, which contained clastic sediments composed of mantle-to crust-derived volcanic rocks (Jiang et al., 2005; Yu et al., 2006; Yang et al., 2011), granites, and metamorphic rocks, then the ore-forming fluid would show a partial mantle signature after water–rock interactions between the basinal fluids and clastic sediments.

## 8. Conclusions

The ore-forming fluids in the South Zhuguang U ore field were sourced primarily from Cretaceous–Paleogene redbed basins in the south, and derived initially from meteoric water. The sediments in these

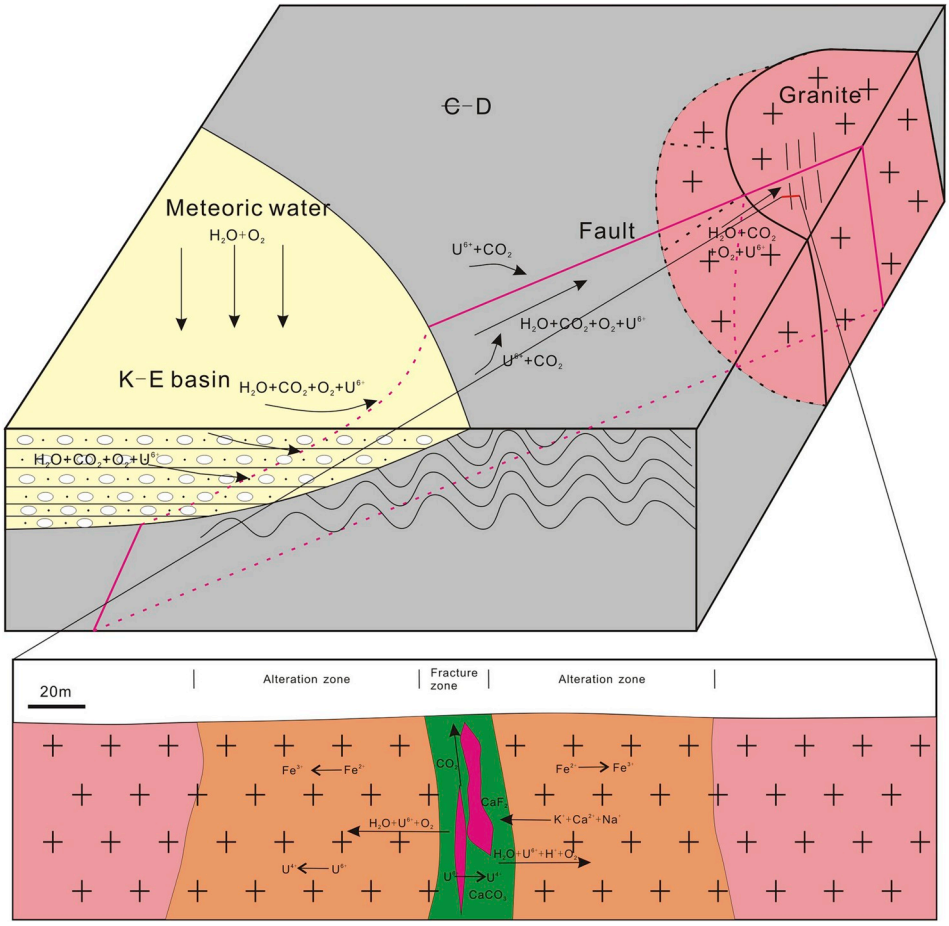


**Fig. 10.** Ore genesis model of the South Zhuguang uranium ore field (Modified from Zhang et al., 2017).

basins were sourced mainly from the surrounding granites and metamorphic rocks. The meteoric water became U- and $CO_2$-bearing through interactions with sediments in the Cretaceous–Paleogene basins, which converted the waters into basinal fluids in terms of H–O–C–S–Sr isotopic compositions. The U-bearing fluids flowed into the Zhuguang granite massif through regional faults, and reacted with the granites adjacent to the faults. The ore-forming fluids can be classified into acidic and oxidizing (stage I), in which fluoride and sulfate complexes of $UO_2^{2+}$ were the dominant species, and alkaline and oxidizing (stage II), in which carbonate and hydroxide complexes of $UO_2^{2+}$ were the dominant species.

During stage I, hydrothermal alteration released considerable amounts of $Ca^{2+}$ and $F^-$ into the ore-forming fluid, increasing its pH, decomposing the dominant fluoride complexes, and lowering the saturation solubility of uranyl. Reduction of the ore-forming fluid led to the conversion of $SO_4^{2-}$ to $S^{2-}$ and $U^{6+}$ to $U^{4+}$, and formation of the pitchblende–fluorite–quartz veins of syn-ore stage I along fractures. During stage II, the U mineralization was controlled mainly by $CO_2$ degassing, which would have decomposed the carbonate complexes ($(UO_2(CO_3)^{2-}$) and resulted in U being precipitated in pitchblende–calcite–quartz veins as the ore-forming fluid became more reduced (Fig. 10).

## Acknowledgement

This research was supported by the National Key R & D Program of Ministry of science and technology of People's Republic of China (Grant No. 2016YFE0206300). The authors sincerely thank Jianji Tian, Yaqing Pang, Ruixiang Hao, and Jialin Liu for their meaningful suggestions.

## Appendix A. Supplementary data

Supplementary data to this article can be found online at https://doi.org/10.1016/j.apgeochem.2018.11.008.

## References

Bernhard, G., Geipel, G., Reich, T., Brendler, V., Amayri, S., Nitsche, H., 2001. Uranyl (VI) carbonate complex formation: validation of the $Ca_2UO_2(CO_3)_3$ (aq.) species. Rediochim. Ac. 89, 511–518.

Bray, C.J., Spooner, E.T.C., Thomas, A.V., 1991. Fluid inclusion volatile analysis by heated crushing, on line gas chromatography; applications to Archean fluids. J. Geochem. Explor. 42, 167–193.

Channer, D.M.DeR., Bray, C.J., Spooner, E.T.C., 1999. Integrated cation-anion/volatile fluid inclusion analysis by gas and ion chromatography; methodology and examples. Chem. Geol. 154, 59–82.

Chen, J.F., Jahn, B.M., 1998. Crustal evolution of southeastern China: Nd and Sr isotopic evidence. Tectonophysics 284, 101–133.

Chen, P.R., Zhang, B.T., Kong, X.G., Cai, B.C., Ling, H.F., Ni, Q.S., 1998a. The geochemical chemical characteristics and their geological implications of the A–type Zhaibei granites, Southern Jiangxi. Acta Petrol. Sin. 14, 163–173 (in Chinese with English Abstract).

Chen, Y.H., Chen, Z.B., Chen, Z.Y., Cai, Y.Q., 1998b. Meso–cenozoic Extensional Tectonics and Uranium Metallogenesis in Southeast China. Atomic Energy Press, Beijing, pp. 1–81 (in Chinese).

CNG (China Nuclear Geology), 2005. Uranium Deposits in South China, Beijing. pp. 1–620 (in Chinese).

CNG (China Nuclear Geology), BRIUG (Beijing Research Institute of Uranium Geology), 2010. The Research and Evaluation of Granite–related Uranium Deposit in China. Beijing. pp. 814–935 (in Chinese).

Clayton, R.N., Friedman, I., Graf, D.L., Mayeda, T.K., Meents, W.F., Shimp, N.F., 1966. The origin of saline formation waters. Isotope Composition. J. Geophys. Res. 71, 3869–3882.

Clayton, R.N., Mayeda, T.K., 1963. The use of bromine pentafluoride in the extraction of oxygen from oxides and silicates for isotopic analysis. Geochem. Cosmochim. Acta 27, 43–52.

Clayton, R.N., O'Neil, J.R., Mayeda, T.K., 1972. Oxygen isotope exchange between quartz

and water. J. Geophys. Res. 77, 3057–3067.
Craig, H., Gordon, L., 1965. Deuterium and oxygen 18 variations in the ocean and the marine atomosphere. In: Symposium on Marine Geochemistry. Graduate school of Oceanography, University of Rhode Island, Occ Publication No 3, pp. 277.
Cuney, M., Brouand, M., Cathelineau, M., Derome, D., Freiberger, R., Hecht, L., Kister, P., Lobaev, V., Lorilleux, G., Peiffert, C., Bastoul, A.M., 2003. What parameters control the high grade-large tonnage of the Proterozoic unconformity related uranium deposits? In: International Conference of Uranium Geochemistry 2003, Proceedings, Nancy, pp. 123–126.
Cuney, M., Kyser, K., 2008. Recent and not–so–recent developments in uranium deposits and implications for exploration. In: Mineralogical Association of Canada, Short Course Series 39, pp. 23–55.
Dahlkamp, J.F., 2009. Uranium Deposits of the World. Springer–Verlag, Berlin Heidelberg, pp. 86–157.
Deng, P., Ren, J.S., Ling, H.F., Shen, W.Z., Sun, L.Q., Zhu, B., Tan, Z.Z., 2011. Yanshanian granite batholiths of Southern Zhuguang Mountain SHRIMP zircon U–Pb dating and tectonic implications. Geol. Rev. 57, 881–888 (in Chinese with English Abstract).
Deng, P., Shen, W.Z., Ling, H.F., Ye, H.M., Wang, X.C., Pu, W., Tan, Z.Z., 2003a. The mantle–drived fluid and uranium mineralization: a case from Xianshi uranium deposit in Xiazhuang uranium orefield. Geochim. 32, 520–528 (in Chinese with English abstract).
Deng, P., Shu, L.S., Tan, Z.Z., 2003b. The Geologic setting for the formation of rich uranium ores in Zhuguang–Guidong large–scale uranium metallogenic area. Geol. Rev. 49, 486–491 (in Chinese with English abstract).
Deng, X.H., Chen, Y.J., Santosh, M., Yao, J.M., 2013. Re–Os geochronology, fluid inclusions and genesis of the 0.85 Ga Tumen molybdenite–fluorite deposit in Eastern Qinling, China: implications for pre-Mesozoic Mo enrichment and tectonic setting. Geol. J. 48, 484–497.
Deng, X.H., Chen, Y.J., Yao, J.M., Bagas, L., Tang, H.S., 2014. Fluorite REE-Y (REY) geochemistry of the ca. 850 Ma Tumen molybdenite–fluorite deposit, eastern Qinling, China: constraints on ore genesis. Ore Geol. Rev. 63, 532–543.
Drummond, S.E., Ohmoto, H., 1985. Chemical evolution and mineral deposition in boiling hydrothermal systems. Econ. Geol. 80, 126–147.
Du, L.T., Wang, Y.M., 1984. The unity of mineralization mechanism of granite–type, volcanic–type, carbonaceous–siliceous–pelite–typeand sandstone–type uranium deposit. Radioactive Geol. 3, 1–10 (in Chinese with English abstract).
Du, L.T., Wang, Y.T., Rong, J.S., Tong, H.C., Li, T.G., Huang, Z.Z., Sun, Z.F., Cai, G.Q., Liu, S.H., Hu, S.K., Li, Y.S., Zhou, W.X., 1982. Contributions of Granite–hosted Uranium Deposits. Atomic Energy Publication House, Beijing, pp. 238–252 (in Chinese with English abstract).
Faure, G., 1986. Principles of Isotope Geology. Wiley, pp. 77–115.
Faure, M., Chen, Y., Feng, Z.H., Shu, L.S., Xu, Z.Q., 2017. Tectonics and geodynamics of South China: an introductory not. J. Asian Earth Sci. 141, 1–6.
Franco, P., 2009. Hydrothermal Processes and Mineral Systems. Springer, Berlin, pp. 73–143.
Gao, F., Lin, J.R., Zhong, Q.L., Guo, S.Y., Pang, Y.Q., Rong, J.S., Hu, Z.H., 2011a. The wall rock alteration and its geochemical characteristics of uranium deposit No. 302. Uranium Geol. 27, 274–281 (in Chinese with English abstract).
Gao, X., Shen, W.Z., Liu, L.L., Yao, W., Zhu, B., Huang, G.L., Li, Q.Y., 2011b. Geochemical characteristics and causes of wall rock alteration in the No. 302 uranium deposit, northern Guangdong. Acta Petrol. Mineral. 30, 71–82 (in Chinese with English abstract).
Gat, J.R., 1984. The stable siotope composition of dead sea waters. Earth Planet Sci. Lett. 71, 361–376.
Gong, W.S., 1990. An approach of Geological characteristics of ore deposit No. 363 and its genesis. Uranium Geol. 6, 77–84 (in Chinese with English Abstract).
Graupner, T., Kempe, U., Spooner, E.T.C., Bray, C.J., Kremenetsky, A.A., Irmer, G., 2001. Microthermometric, laser Raman spectroscopic, and volatile-ion chronmatographic analysis of hydrothermal fluids in the paleozoic muruntau Au-bearing quartz vein ore field. Uzbekistan. Econ. Geol. 98, 1–23.
Guangdong, BGMR (Bureau of Geology and Mineral Resources of Guangdong Province), 1988. In: Regional Geology of the Guangdong Province. Geological Publishing House, Beijing, pp. 1–941 (in Chinese with English abstract).
Hoefs, J., 1997. Stable Isotope Geochemistry. Springer, Berlin, pp. 27–118.
Horite, J., Wesolowski, D.J., 1994. Liquid–vapor fractionation of oxygen and hydrogen isotopes of water from the freezing to the critical temperature. Geochem. Cosmochim. Acta 58, 3425–3437.
Hu, R.Z., 1984. The Metallogenetic Geophysical and Geochemical Conditions and Genetic Discussion of No.302 Deposit. M.S thesis. Chengdu College of Geology, Chengdu, pp. 1–87 (in Chinese with English abstract).
Hu, R.Z., Bi, X.W., Zhuo, M.F., Peng, J.T., Su, W.C., Liu, S., Qi, H.W., 2008. Uranium metallogenesis in south China and its relationship to crustal extension during the cretaceous to tertiary. Econ. Geol. 103, 583–598.
Hu, R.Z., Burnard, P.G., Bi, X.W., Zhou, M.F., Peng, J.T., Su, W.C., Zhao, J.H., 2009. Mantle-derived gaseous components in ore-forming fluids of the Xiangshan uranium deposit, Jiangxi Province, China: evidence from He, Ar and C isotopes. Chem. Geol. 266, 86–95.
Hu, R.Z., Li, C.Y., Ni, S.J., Liu, L., Yu, J.S., 1993. Research on $\Sigma CO_2$ source in ore–forming hydrothermal solution of granite type uranium deposits, South China. Sci. China (D) 36, 1252–1262 (in Chinese).
Huang, G.L., Yin, Z.P., Ling, H.F., Deng, P., Zhu, B., Shen, W.Z., 2010. Formation age, geochemical characteristics and genesis of pitchblende from No.302 uranium deposit in northern Guangdong. Miner. Deposits 29, 352–360 (in Chinese with English abstract).
Huang, J.B., Huang, S.J., Zhang, J.D., Li, Y.L., Han, C.Q., 2005. The Uranium Belts in China. China Nuclear Geology, Beijing, pp. 65–143 (in Chinese).
Huang, J.P., 1996. The stable isotopic characteristics of uranium deposit No.211. Comput. Tech. Geophys. Geochem. Explor. 18, 47–49 (in Chinese with English abstract).
Hunan, BGMR (Bureau of Geology and Mineral Resources of Hunan Province), 1988. Regional Geology of the Hunan Province. Geological Publishing House, Beijing, pp. 286–507 (in Chinese with English abstract).
Jiang, Y.H., Ling, H.F., Jiang, S.Y., Fan, H.H., Zhou, W., Ni, P., 2005. Petrogenesis of a Late Jurassic Peraluminous volcanic complex and its high-Mg, potassic, quenched enclaves at Xiangshan, Southeast China. J. Petrol. 46, 1121–1154.
Jiangxi, BGMR (Bureau of Geology and Mineral Resources of Jiangxi Province), 1984. Regional Geology of the Jiangxi Province. Geological Publishing House, Beijing, pp. 1–921 (in Chinese with English abstract).
Jin, J.F., Liu, A.P., 1993. Characteristics of granites and sources of Uranium in No. 316 Uranium deposit. Miner. Deposits 12, 253–264 (in Chinese with English abstract).
Kojima, S., Takeda, S., Kogita, S., 1994. Chemical factors controlling the solubility of uraninite and their significance in the genesis of unconformity–related uranium deposits. Miner. Deposits 29, 353–360.
Kyser, T.K., Hiatt, E., Renac, C., Durocher, K., Holk, G., Deckart, K., 2000. Diagenetic fluids in paleo-and meso-proterozoic sedimentary basins and their implications for long protracted fluid histories. In: Kyser, T.K. (Ed.), Fluid and Basin Evolution, Short Course 28. Miner. Assoc, Canada, pp. 225–262.
Kyser, T.K., O'Neil, J.R., 1984. Hydrogen isotope systematics of submarine basalts. Geochem. Cosmochim. Acta 48, 2123–2134.
Langmuir, D., 1978. Uranium solution–mineral equilibria at low temperatures with applications to sedimentary ore deposits. Geochem. Cosmochim. Acta 42, 547–569.
Li, C.J., Jiang, X.L., 1992. Metallogenetic model for two types of fluorite deposits in Southeastern China. Acta Geol. Sin. 5, 75–88.
Li, T.G., 1989. Geological features of deposits No.201 and No. 361 and analyses of formation conditions of uranium–rich ore deposits. Uranium Geol. 5, 66–71 (in Chinese with English abstract).
Li, T.G., Tong, H.S., Feng, M.Y., 1996. Geological characteristics and formation conditions of rich ore in granitic type uranium deposits. In: In: Chen (Ed.), Galaxy of Research Achievements of Uranium Geology of China, vol. 12. Uranium Geol., pp. 122–131 (in Chinese with English Abstract).
Li, X.H., 1992. Petrogenesis of zhuguangshan mesozoic granites. Guangdong Geol. 7, 1–13 (in Chinese with English Abstract).
Li, X.H., Hu, R.Z., Rao, B., 1997. Geochronology and geochemistry of cretaceous mafic dikes in north Guangdong province. Geochem. 26, 14–31 (in Chinese with English Abstract).
Li, Y.X., 1990. A study of the wall–rock alteration geochemistry in rich uranium deposit No.201. Uranium Geol. 6, 359–368 (in Chinese with English abstract).
Li, Y.X., Li, T.G., Tong, H.S., Feng, M.Y., Xu, Z., 1995. A study on Hydrogen, Oxygen, Carbon, Sulfer and Lead isotopes in the rich uranium deposit No.201. Uranium Geol. 11, 273–301 (in Chinese with English abstract).
Li, Z.Y., 2006. Hotspot uranium metallogenesis in South China. Uranium Geol. 22, 64–69 (in Chinese with English abstract).
Liu, A.P., Jin, J.F., 1993. The features of structural ore–control in Uranium deposit 361. J. Chengdu Coll. Geol. 20, 106–112 (in Chinese with English abstract).
Liu, A.P., Jin, J.F., 1994. The hydrothermal geochemical features and physico–chemical conditions of uranium deposit 361. J. Chengdu Coll. Geol. 21, 51–61 (in Chinese with English abstract).
Luo, J.C., Hu, R.Z., Fayek, M., Li, C.S., Bi, X.W., Abdu, Y., Chen, Y.W., 2015. In–situ SIMS uraninite U–Pb dating and genesis of the Xianshi granite–hosted uranium deposit, South China. Ore Geol. Rev. 65, 968–978.
Maynard, J.B., 1991. Shale-Hosted deposits of Pb, Zn, and Ba: syngenetic deposition from exhaled brines in deep marine basins. In: In: Force (Ed.), Sedimentary and Diagenetic Mineral Deposits: a Basin Analysis Approach to Exploration, vol. 5. Rev. Econ. Geol., pp. 177–185.
Mccrea, J.M., 1950. The isotopic chemistry of carbonates and a paleotemperature scale. J. Chem. Phys. 18, 849–857.
McKibben, M.A., Eldridge, C.S., 1990. Radical sulfur isotope zonation of pyrite accompanying boiling and epithermal gold deposition. Econ. Geol. 85, 1917–1925.
Min, M.Z., Fang, C.Q., Fayek, M., 2005. Petrography and genetic history of coffinite and uraninite from the Liueryiqi granite–hosted uranium deposit, SE China. Ore Geol. Rev. 26, 187–197.
Min, M.Z., Luo, X.Z., Du, G.S., He, B.A., Camphell, A.R., 1999. Mineralogical and geochemical constraints on the genesis of the granite–hosted Huangao uranium deposit,SE China. Ore Geol. Rev. 14, 105–127.
Nakamura, N., Tatsumoto, M., Nunes, P.D., Unruh, D.M., Schwab, A.P., Wildeaman, T.R., 1976. 4.4 y–old clast in Boulder 7, Apollo 17: a comprehensive chronological study by U–Pb, Rb–Sr and Sm–Nd methods. In: Proceedings of 7th Lunar Scientific Conference, pp. 2309–2333.
Ohmoto, H., Rye, R.O., 1979. Isotopes of sulfur and carbon: geochemistry of hydrothermal ore deposits. In: Barnes, H.L. (Ed.), Geochemistry of Hydrothermal Ore Deposits, second ed. Wiley, New York, pp. 509–567.
Ohmoto, H., 1972. Systematics of sulfur and carbon isotopes in hydrothermal ore deposits. Econ. Geol. 67, 551–578.
Ohmoto, H., Goldhaber, M.B., 1997. Sulfur and carbon isotopes. In: Barnes, H.L. (Ed.), Geochemistry of Hydrothermal Ore Deposits, third ed. Wiley, New York, pp. 517–612.
O'Neil, J.R., Clayton, R.N., Mayads, T.K., 1969. Oxygen isotope fractionation in divalent metal carbonates. J. Chem. Phys. 51, 5547–5558.
Robb, L., 2005. Introduction to Ore–forming Processes. Blcakwell Publishing Company, Oxford, pp. 166–168.
Robinson, B.W., Kusakabe, M., 1975. Environment of deposition of stratiform Mississippi Valley–type ore deposits, from studies of fluid inclusions. Econ. Geol. Monogr. 3, 349–362.

Romberger, S.B., 1984. Transport and deposition of uranium in hydrothermal systems at temperatures up to 300°C, with genetic implications. Geology of uranium deposits, Special Volume, Canadian Ins. Min. Metall. 32, 12–17.
Sheppard, S.M.F., 1986. Characterization and isotopic variations in natural waters. In: stable isotopes in high temperature geological processes. Rev. Mineral. Geochem. 16, 165–183.
Shu, L.S., Deng, P., Wang, B., Tan, Z.Z., Yu, X.Q., Sun, Y., 2004. The late mesozoic mountain–basin evolution in nanxiong–zhuguang area: constraints from petrology, kinematics, and geochronlogy. Sci. China (D) 34, 1–13 (in Chinese).
Shu, X.J., 2004. Application of gravimetric and aeromagnetic data to the study of uranium ore–formation of granite–type uranium deposits. Uranium Geol. 20, 99–119 (in Chinese with English Abstract).
Sofer, Z., Gat, J.R., 1975. The isotopic composition of evaporating brines: effect of the isotopic activity ratio in saline solutions. Earth Planet Sci. Lett. 26, 179–186.
Sun, L.Q., Ling, H.F., Shen, W.Z., Huang, G.L., Tan, Z.Z., 2010. Geochronology of youshan and pingtian granites in nanling range and its geological implications. Geol. J. China Univ. 16, 186–197 (in Chinese with English Abstract).
Taylor, H.P., 1974. The application of oxygen and hydrogen isotope studies to problems of hydrothermal alteration and ore deposition. Econ. Geol. 69, 843–883.
Tripathi, V.S., 1979. Comments on "Uranium solution–mineral equilibria at low temperatures with applications to sedimentary ore deposits. Geochem. Cosmochim. Acta 43, 1989–1990.
Wan, T.F., 2004. The Tectonics of China. Geological Publishing House, Beijing, pp. 135–213 (in Chinese).
Wang, D.H., Li, H.Q., Qu, W.J., He, H.H., Qin, Y., Liu, X.X., Huang, F., Wang, C.H., Li, C., Chen, Z.H., Li, J.K., Zhang, C.Q., Wang, Y.L., Mei, Y.P., Ying, L.J., Li, L.X., Zhao, Z., Zhao, Z., Fu, Y., Sun, T., Hou, K.J., 2014. The Diagenetic and Mineralization Ages of Deposits in China. Geological Publication House, Beijing, pp. 1–364 (in Chinese).
Wang, M.T., Luo, Y., Sun, Z.F., Zhu, J.C., Li, J.H., 1999. Discussion on genesis of uranium deposits in Zhuguang uranium metallogenic region. Uranium Geol. 15, 279–285 (in Chinese with English abstract).
Wu, Q.S., 1985. Rb–Sr ages of some moderately–weakly metamorphosed rocks in South China. Geotech. Metall. 24, 245–262 (in Chinese with English abstract).
Yang, S.Y., Jiang, S.Y., Jiang, Y.H., Zhao, K.D., Fan, H.H., 2011. Geochemical, zircon U-Pb dating and Sr-Nd-Hf isotopic constraints on the age and petrogenesis of an Early Cretaceous volcanic-intrusive complex at Xiangshan, Southeast China. Mineria Pet. 101, 21–48.
Yu, X.Q., Wu, G.G., Zhang, D., Yan, T.Z., Di, Y.J., Wang, L.W., 2006. Cretaceous extension of the Ganhang Tectonic Belt, southeastern China: constraints from geochemistry of volcanic rocks. Cretac. Res. 27, 663–672.
Zhang, C., Cai, Y.Q., Xu, H., Dong, Q., 2018a. Genesis of South Zhuguang uranium ore field, south China: constraints from the mineralization ages and Pb isotope. Resour. Geol. https://doi.org/10.1111/rge.12184.
Zhang, C., Cai, Y.Q., Xu, H., Dong, Q., Liu, J.L., Hao, R.X., 2017. The mineralization mechanism of Changjiang Uranium Ore Field, South China: evidence from fluid inclusion, hydrothermal alteration, and H–O isotopes. Ore Geol. Rev. 86, 225–253.
Zhang, G.Q., 2008. Geochemistry of Hydrothermal Uranium Deposits in South China:A Case Study of the No.302 Uranium Deposit. Ph.D dissertation. Chinese Academy of Sciences, Guiyang, pp. 1–120 (in Chinese with English Abstract).
Zhang, G.Q., Hu, R.Z., Shang, P.Q., Tian, J.J., Shuang, Y., 2008. Study on the C-O isotopic composition of calcites and Metallogenic dynamics background in the No.302 uranium deposit. Acta Mineral. Sin. 28, 413–420 (in Chinese with English abstract).
Zhang, L., Chen, Z.Y., Li, X.F., Li, S.R., Santosh, M., Huang, G.L., 2018b. Zircon U-Pb geochronology and geochemistry of granites in the Zhuguangshan complex, South China: implications for uranium mineralization. Lithos 308 (309), 19–33.
Zhang, L.G., Chen, Z.S., Liu, J.X., Yu, G.X., Wang, K.F., Wang, B.C., Xu, J.F., Zheng, W.S., Li, D.Y., Li, H., Hou, D.Y., 1995. Isotopic Exchange Theories of Two Stages during Water-rock Reaction, and Their Applications in Exploration. Geological Press, Beijing, pp. 14–41.
Zhang, Z.S., Hua, R.M., Deng, P., Zhu, B., Wu, L.Q., Zhang, Y.C., Tan, Z.Z., Yin, Z.P., 2005. Geological and geochemical characteristics of water–rock interaction in the processes of uranium mineralization in Zhuguang–Xiazhuang uranium ore–concentrated district. Geochim. 34, 483–494 (in Chinese with English Abstract).
Zhang, Z.S., Hua, R.M., Ji, J.F., Zhang, Y.C., Guo, G.L., Yin, Z.P., 2007. Characteristics and formation conditions of chlorite in No. 201 and No. 361 uranium deposit. Acta Mineral. Sin. 27, 161–172 (in Chinese with English abstract).
Zhao, K.D., Jiang, S.Y., Dong, C.Y., Chen, W.F., Chen, P.R., Ling, H.F., Zhang, J., Wang, K.X., 2011. Uranium bearing and barren granites from the Taoshan complex, Jiangxi Province, South China: geochemical and Petrogenetic discrimination and exploration significance. J. Geochem. Explor. 110, 126–135.
Zhao, K.D., Jiang, S.Y., Ling, H.F., Sun, T., Chen, W.F., Chen, P.R., Pu, W., 2016. Late Triassic U–bearing and barren granites in the Miao'ershan batholith, South China: petrogenetic discrimination and exploration significance. Ore Geol. Rev. 77, 260–278.
Zheng, Y.F., Chen, J.F., 2000. Stable Isotope Geochemistry. Science Press, Beijing, pp. 38–109.
Zheng, Y.F., Hoefs, J., 1993. Effects of mineral precipitation on the sulfur isotope composition of hydrothermal solutions. Chem. Geol. 105, 259–269.
Zhou, W.X., 1996. Continental tectonics and uranium province of south China. In: Chen (Ed.), Galaxy of Research Achievements of Uranium Geology of China. Beijing, China Nuclear Geology, pp. 26–34 (in Chinese).
Zhou, W.X., Zhang, B.T., Wu, J.H., 2003. Granite types uranium deposits in south China uranium province. In: Cuney (Ed.), Uranium Geochemistry. Univ Henri Poincaré, Vandoevre les Nancy, pp. 396–399.